



## Lava flow hazard map of Piton de la Fournaise volcano

Magdalena Oryaëlle Chevrel<sup>1</sup>, Massimiliano Favalli<sup>2</sup>, Nicolas Villeneuve<sup>3,4,5</sup>, Andrew J. L. Harris<sup>1</sup>,  
Alessandro Fornaciai<sup>2</sup>, Nicole Richter<sup>3,5,6</sup>, Allan Derrien<sup>3,5</sup>, Patrice Boissier<sup>3,5</sup>, Andrea Di Muro<sup>3,5</sup>, Aline  
Peltier<sup>3,5</sup>

- 5 <sup>1</sup>Université Clermont Auvergne, CNRS, IRD, OPGC, Laboratoire Magmas et Volcans, F-63000 Clermont-Ferrand, France.  
<sup>2</sup>Istituto Nazionale di Geofisica e Vulcanologia (INGV), Via Battisti, 53, 56125 Pisa, Italy.  
<sup>3</sup>Université de Paris, Institut de physique du globe de Paris, CNRS, F-75005 Paris, France.  
<sup>4</sup>Université de La Réunion, Laboratoire Géosciences Réunion, F-97744 Saint-Denis, France.  
<sup>5</sup>Observatoire Volcanologique du Piton de la Fournaise, Institut de physique du globe de Paris, F-97418 La Plaine des Cafres,  
10 France.  
<sup>6</sup>Helmholtz Centre Potsdam, German Research Centre for Geosciences (GFZ), Telegrafenberg, Potsdam, 14473, Germany

*Correspondence to:* Magdalena Oryaëlle Chevrel (oryaelle.chevrel@ird.fr)

**Abstract.** Piton de la Fournaise, situated on La Réunion Island (France), is one of the most active hot spot basaltic shield  
volcanoes worldwide, experiencing at least two eruptions per year since the establishment of the observatory in 1979. Eruptions  
15 are typically fissure-fed and form extensive lava flow fields. About 95 % of some ~250 historical events (since the first  
confidently dated eruption in 1708) have occurred inside an uninhabited horse-shoe shaped caldera (hereafter referred to as  
the Enclos) which is open to the ocean on its eastern side. Rarely (12 times since the 18<sup>th</sup> century), fissures have opened outside  
of the Enclos where housing units, population centers and infrastructure are at risk. In such a situation, lava flow hazard maps  
are a useful way of visualizing lava flow inundation probabilities over large areas. Here, we present a lava flow hazard map  
20 for Piton de la Fournaise volcano based on: i) vent distribution, ii) statistics of lava flow lengths, iii) lava flow recurrence  
times, and iv) simulations of lava flow paths across multi-temporal (i.e., regularly updated) topography using the  
DOWNFLOW stochastic numerical model. A map of the entire volcano highlights that the most probable (up to 12 %) location  
for future lava flow inundation is within the Enclos, where about 100,000 visitors are present each year. Hazard distribution  
changes throughout the analysis period due to the high frequency of eruptions that constantly modifies the vent opening  
25 distribution as well as the topography and the lava flow dimensional characteristics. Outside of the Enclos, probabilities reach  
0.5 % along the well-defined rift zones and, although hazard occurrence in inhabited areas is deemed to be very low (<0.1 %),  
it may be underestimated here, as our study is only based on post-18<sup>th</sup> century records and neglects cycles of activity at the  
volcano. Specific hazard maps considering different event scenarios (i.e., events fed by different combinations of temporally  
evolving superficial and deep sources) are required to better assess affected areas in the future – especially by atypical, but  
30 potentially extremely hazardous, large volume eruptions. At such an active site, our method supports the need for regular  
updates of DEMs and associated lava flow hazard maps if we are to be effective in mitigating the associated risks.



## 1 Introduction

Lava flow hazard maps represent the probability of inundation by a lava flow per unit area. Because such maps show areas that are at the highest risk, it is a fundamental tool in lava flow hazard mitigation and in guiding eruption response management. Lava flow hazard maps for basaltic volcanic centers have been previously produced for several highly active volcanoes including Mount Etna in Italy (Favalli et al., 2005; Favalli et al., 2011; Del Negro et al., 2013), Nyiragongo in the Democratic Republic of Congo (Chirico et al., 2009; Favalli et al., 2009), and Mount Cameroon in the Cameroon (Bonne et al., 2008; Favalli et al., 2012). They have also been produced for most ocean island basaltic shields including Mauna Loa and Kilauea on the island of Hawaii (Kauahikaua et al., 1998; Rowland et al. 2005), Lanzarote in the Canaries, Spain (Felpeto et al., 2001), Pico in the Azores, Portugal (Cappello et al., 2015), Fogo in Capo Verde (Richter et al. 2016), and Karthala in the Grande Comore (Mossoux et al., 2019). Having been active with an eruption every nine months since the beginning of the 20<sup>th</sup> century (Michon et al., 2013), producing such a map for Piton de la Fournaise (La Réunion, France) is a particularly pressing need. At the same time, the wealth of data for eruptive events at Piton de la Fournaise means that we can use this location as a case study to further test, develop and evolve methods for effective lava flow hazard map preparation at frequently active effusive centers.

Following widespread damage due to lava ingress into the town of Piton Sainte Rose in 1977, a volcano observatory (the *Observatoire Volcanologique du Piton de la Fournaise*, OVPF managed by the *Institut de Physique du Globe de Paris*,) was established on Piton de la Fournaise in 1979. The objective was to ensure an adequate monitoring network and surveillance, thereby improving hazard mitigation. Today, the permanent monitoring network run by OVPF is one of the densest in the world, comprising more than 100 stations including seismometers, tiltmeters, extensometers, GNSS receivers, gas monitoring stations, cameras and weather stations. This network allows OVPF to detect eruption onset and provide early warning to authorities so that they can organize implementation of the nationally-mandated response plan to be followed by civil protection (the “ORSEC-DSO plan”), a plan which includes provision for evacuation of volcano visitors and resident populations if needed (Peltier et al., 2018, 2020). However, effective hazard management also requires preparation of hazard maps to guide mitigation measures and actions (Pallister et al., 2019). In this regard, an exhaustive database for eruptive events has been built by OVPF through their response to 77 eruptions between 1979 and 2019, all of which have been geophysically, petrographically and physically mapped and measured. The existence of such a data base allows application of a robust empirical approach to hazard mapping and planning (Pallister et al., 2019). Currently this data base includes:

- i) An exhaustive lava flow inventory based on detailed mapping over the period 1931–2019 (Derrien, 2019; Staudacher et al., 2016; OVPF database) coupled with lava flow dating (Albert et al., 2020) that allows estimation of the lava flow recurrence time;
- ii) Three high-spatial (25 to 1 m) resolution Digital Elevation Models (DEMs) acquired in 1997, 2010 and 2016 (Arab-Sedze et al., 2014; Bretar et al., 2013; Derrien, 2019);



65           iii)       A complete data base for vent distribution (up to the end of 2019) to allow robust calculation of the probability density function of future vent opening (Favalli et al., 2009a).

At Piton de la Fournaise, the impact of lava flow hazard has previously been studied by Villeneuve (2000) and Davoine and Saint-Marc (2016), and an initial lava flow hazard map was published in a national report in 2012 (Di Muro et al., 2012). This map is also mentioned in Nave et al. (2016). However, the hazard map was drafted based on a topography acquired in 1997, and between the publication of the national report in 2012 and the end of 2019, eighteen eruptions occurred resurfacing approximately 19 km<sup>2</sup> of land. Thus, regular reassessments of lava flow hazard at Piton de la Fournaise are needed to allow regular updates of maps in this highly active environment where topography is changing annually due to emplacement of new lava flow units. Mapping also needs to be flexible and reactive to the changing hazard situation as new vents and vent distributions become established (Favalli et al., 2009a), and the style, magnitude and intensity of effusive volcano activity evolves (Harris and Rowland, 2009; Keszthelyi and Self, 1998).

70           To build a hazard map in a such this dynamic environment we employed the DOWNFLOW code of Favalli et al. (2005), this being a stochastic model that allows quick, computationally efficient and flexible estimation of the most probable areas to be covered by lava flows (e.g., Favalli et al., 2009b, 2011; Richter et al., 2016). To apply DOWNFLOW, we need to calibrate it by obtaining the best-fit parameters to reproduce the area of lava flow coverage for selected flows. Building a hazard map, also involves calculation of the lava flow temporal recurrence intervals, as well as vent distributions (Favalli et al., 2009a). We here describe this methodology, step-by-step, and present the resulting up-to-date lava flow hazard map for Piton de la Fournaise. Additionally, we compare the three hazard maps derived from the three DEMs acquired in 1997, 2010 and 2016 to assess and discuss the effectiveness of this method, and the evolution of the hazard maps resulting from changes in the DEMs; as will occur, at frequently active basaltic volcanoes. First, though, we present the morphological setting and eruptive activity at Piton de la Fournaise so as to define the hazard and risk scenarios for this case type example.

### 85           1.1. Morphological setting

La Réunion island is located in the western Indian Ocean, around 700 km east of Madagascar and 180 km southwest of Mauritius. The island is composed of two large shield volcanoes (Fig. 1a): Piton des Neiges, which is considered dormant, and Piton de la Fournaise which is one of the most active volcanoes in the world (Peltier et al., 2009; Roult et al., 2012). The Piton de la Fournaise edifice is marked by a large horse-shoe shaped caldera, referred to hereafter by its local name “the Enclos” (French for “enclosure”). The Enclos is a 8 km wide structure, which is open to the ocean to the east and is surrounded by cliffs of up 100 m high to the west, north and south (Fig. 1b). This morphology contains any active lava flow to the Enclos limits, with the west to east slope guiding flow towards the ocean. Although it is commonly accepted that the Enclos is the most recent collapse structure at Piton de la Fournaise, its mechanisms of formation and respective ages are still debated. While it may have been formed by a series of collapses and successive landslides (Bachèlery 1981; Merle et al., 2010; Michon and Saint-Ange, 2008; Merle and Lénat, 2003), it may also be the result of only landslides (Duffield et al., 1982; Gillot et al. 1994; Oehler et al. 2004, 2008). The upper part of the Enclos, whose western plateau is located at >1800 m a.s.l., is recognized here



as the caldera *sensu stricto* (Michon and Saint-Ange, 2008) and is named the Enclos Fouqué (EF) (Fig. 1b). It is a relatively flat plateau in the middle of which an asymmetric terminal shield has been built to reach an altitude of 2632 m a.s.l. and with slopes of between 15° (on the northern flank) and 30° (on the eastern flank). The top of the terminal shield is marked by a 1.1 × 0.8 km summit caldera (“Cratère Dolomieu”) that last collapsed in 2007 (Michon et al., 2009; Staudacher et al., 2009; Derrien et al., 2020). To the west, Cratère Dolomieu coalesces with a smaller (0.38 × 0.23 km) crater (“Cratère Bory”). The eastern part of the Enclos, i.e., below 1800 m a.s.l., is divided into two areas (most probably formed by successive landslides; Michon and Saint-Ange, 2008) where the slopes are very steep (>30°), hereafter named “Grandes Pentès” (French for “steep slopes”), and the flatter coastal area, hereafter named “Grand-Brûlé” (French for “widely-burned”; Fig. 1b).

## 1.2 Effusive activity and risk

As observed on most basaltic shield volcanoes (Dvorak et al., 1983; Tilling and Dvorak, 1993; Walker, 1988), eruptions at Piton de la Fournaise are produced by dyke/sill propagation following preferential paths leading to the concentration of eruptive fissures within, tangential-to or radially-around the summit crater and along three main rift zones (Bachèlery, 1981). At Piton de la Fournaise, there are three rift zones, the southeast rift zone (SERZ), the northeast rift zone (NERZ) and the north 120° rift zone (N120), and these are the zones where effusive activity is mainly concentrated (Fig. 1b). Two other zones with a high concentration of eruptive fissures have also been identified, these being the South Volcanic Zone (SVZ) and the Puy Raymond Volcanic Alignment (PRVA; Michon et al. 2015; Fig. 1b).

Eruptions are mainly effusive and expressed fed by en-echelon fissure sets, with each fissure being a few meters to a few hundred meters long. Activity at the fissures tends to be Hawaiian to Strombolian in style, to feed lava flows that can extend all the way to the ocean, a distance of up to 12 km downslope (cf. Sect. 6). The average volume of lava emitted per eruption between 1970 and 2007 was about  $10 \times 10^6 \text{ m}^3$  (Peltier et al., 2009). In 2007, activity was punctuated by a low-elevation flank (590 m a. s. l.) event in the Enclos, during which  $140 \text{ to } 240 \times 10^6 \text{ m}^3$  of lava was erupted in 30 days (Roult et al., 2012; Staudacher et al., 2009). Such atypical “low flank” events can be of high risk (Lormand et al., 2020), and historically the 2007 event has been, volumetrically, the largest single effusive event witnessed at Piton de la Fournaise. Through April 2020, it has been followed by a further 28 more “typical” eruptions, each with a typical volume of  $5 \times 10^6 \text{ m}^3$  and being fed from vents at higher altitudes (OVPF reports ISSN 2610-5101). Lava flows can be channel fed (e.g., Harris et al., 2016; Rhéty et al., 2017; Soldati et al., 2018), to feed extensive compound lava flow fields within the Enclos (Fig. 1b), although tubes can form during longer-lived eruptions, as in 2007 (Staudacher et al., 2009). Lava composition is usually transitional, ranging from aphyric basalt to oceanite and midalkaline basalt (Albarède et al., 1997; Lénat et al., 2012), with eruption temperatures in the range 1150-1190 °C (e.g., Boivin and Bachèlery, 2009; Harris et al., 2019; Di Muro et al., 2014). Lavas thus have a relatively low viscosity of the order of  $10^2\text{--}10^4 \text{ Pa s}$  upon eruption (Harris et al., 2016; Kolzenburg et al., 2018; Rhéty et al., 2017).

Most effusive eruptions at Piton de la Fournaise occur within the Enclos. This is part of La Réunion National Park and is uninhabited. However, being a major tourist attraction, the Enclos does receive about one hundred thousand visitors per



year. As a result the hiking trails in, and access roads to, the Enclos can receive heavy pedestrian and vehicular traffic (e.g., 129 000 hikers accessed the summit in 2011 according to Derrien et al., 2018). The Enclos also hosts the national road (RN2) which crosses the Enclos from north to south at a distance of 800 m inland from the coast and at an altitude of 130-70 m a.s.l. (Fig. 1b). This is the island belt road and, if cut, severely impedes communications and travel between communities in the south and north of the island (Harris and Villeneuve, 2018). Based on an analyses of the records available since the first observation in 1640, Villeneuve and Bachèlery (2006) estimated that 95 % of the eruptions have occurred in the Enclos Fouqué caldera (i.e., above 1800 m a.s.l.). These are, hereafter, termed “proximal” eruptions as they are proximal to the terminal shield. Fissures and associated lava flows produced by these proximal eruptions may cut hiking trails and generate a risk for the visitors (Derrien et al., 2018), and necessitates evacuation and closure of the Enclos (Peltier et al., 2020). Fissures may also open on the Grandes Pentes or in the Grand-Brûlé, i.e., below 1800 m a.s.l.. These are termed “distal” eruptions and these can cut the RN2, as has been the case for eight eruptions since 1979 (Fig. 1b). Eruptions outside of the Enclos, termed *Hors Enclos* eruptions – “hors” being French for outside, are high risk as they can open in or above inhabited areas near the coast, such as above the villages of Sainte-Rose and Saint-Philippe (Fig. 1b). They can also open in the inhabited highlands of the volcano, where there are the towns of La Plaine des Cafres and Plaines des Palmistes (Fig. 1b). For example, the eruption of April 1977, which was the first *Hors Enclos* eruption since 1800, caused evacuation of Piton Sainte-Rose, burnt down or damaged parts of 26 buildings (including houses, a church, the police station and a gas station) and buried part of the Sainte-Rose municipality (Kieffer et al., 1977). A second *Hors Enclos* eruption in March 1986 caused around 400,000 euros of damage to houses, household contents, agriculture, roads and utilities in the municipality of Sainte Phillippe (Bertile, 1987; Morin, 2012).

### 1.3 Cycles of effusive activity

At Piton de la Fournaise, the location and frequency of effusive activity is controlled by the shallow (<2.5 km below the summit) stress field. According to Peltier et al. (2009), Got et al. (2013) and Derrien (2019), the evolution of the stress field at Piton de la Fournaise can follow cycles that have typical periods of one year to slightly more than a decade. These cycles typically start with one or a few eruptions at the summit, followed by one or a few proximal eruptions (with vents opening on the terminal shield or at its base). They may end with a large-volume, distal eruption at a distance of more than 4 km from the summit, as was the case in 2007, or an *Hors Enclos* eruption, as was the case for the cycle that ended in 1977. In addition to these superficial cycles, lava composition seems to be affected by cyclic changes in the “fertility” of the source magma as observed since 1930, the date since which the petrology of the volcanic products has been well documented (Vlastélic et al., 2018). These deep source-related cycles are typically of longer duration (20–30 years) and are characterized by a continuous increase followed by a continuous decrease in source fertility, until a minima is reached which marks the end of a cycle and the beginning of a new one (Vlastélic et al., 2018). High-volume distal eruptions associated to crater collapse occurring in 1931-35, 1961, 1986 and 2007 mean that three-quarters of such cycles are characterized by such “atypical”, low flank events, where they typically occur just after the peak of source fertility (Derrien, 2019). This cyclic activity shows that eruptive fissures



are more likely to open at lower altitudes and outside of the Enclos towards the end of superficial cycles, and particularly  
165 voluminous effusive events may be expected just after the peak in a deep-seated cycle.

## 2 Digital Elevation Models

Given the sensitivity of lava flow paths to topography (Favalli et al., 2005), for a target where the topography changes so often  
as is the case at Piton de la Fournaise, using a frequently updated, and indeed up-to-date, Digital Elevation Model (DEM) is  
essential. For this study we could use to three DEMs. The first was obtained in 1997 for the whole island as derived from SIR-  
170 C images. This DEM has a vertical and horizontal resolution of 0.15 m and 25 m, respectively, and was available on a local  
projection (Gauss-Laborde Réunion) where elevations were based on the ellipsoid (Villeneuve, 2000). The second DEM was  
acquired in 2008-2009 by airborne Light Detection And Ranging (LIDAR) and has a 5 m resolution over the whole island,  
and 1 m resolution near the coast. The vertical resolution is 0.05 to 0.1 m (Arab-Sedze et al., 2014). Finally, the most recent  
DEM was obtained in April 2016 from optical Pléiades satellite images acquired in Stereo Triplet mode and processed by the  
175 *French Centre National d'Etudes Spatiales* using their S2P restitution code (de Franchis et al., 2014). This DEM is restricted  
to the Enclos, which is where all topographic changes took place between 2009 and 2016, and was sampled at 5 m resolution  
for this study.

## 3 Lava flow recurrence time

As a first step in building our lava flow hazard map, we needed to prepare a complete and statistically robust eruption  
180 inventory, to estimate lava flow recurrence time on the volcano flank. The inventory of all eruptions since record allows  
(beginning of the 18<sup>th</sup> century since the first confidently dated eruption in 1708) has been detailed by several studies (Michon  
et al., 2013; Morandi et al., 2016; Villeneuve and Bachèlery, 2006). By compiling these studies and the exhaustive record since  
establishment of the OVPF (Peltier et al., 2009; Roult et al., 2012; Vlastélic et al., 2018), as well as recent OVPF reports (ISSN  
2610-5101), we estimate that Piton de la Fournaise had about 250 eruptive events over a period of three centuries. About 95  
185 % of these have occurred inside the Enclos (Table S1).

To produce the lava flow hazard map, we need to account for recurrence of lava flows and not the number of eruptive  
events. Moreover, an eruptive event may produce several lava flows that can be located several kilometers apart. Therefore,  
an individual flow is counted when it is either temporally or spatially separated from another flow. Therefore, an individual  
flow is counted and entered into the data base when it is either temporally or spatially separated from another flow. For any  
190 eruption at Piton de la Fournaise a fissure typically opens perpendicular to the slope, the magma erupts uniformly along the  
fissure to feed several lava flow units simultaneously to form a flow field of many overlapping flow units. In such a case we  
count only a single flow, the longest, and do not consider all units that comprise the compound lava flow field in the data base  
(e.g., Walker, 1973). In the case where there is a pause in the eruption and new flows are emitted in a second phase of activity,



then the longest flow after the hiatus is also counted, so that the eruption has two flows associated with it in the data base.  
195 Finally, if an eruption feeds lava flows at multiple, spatially distinct locations, each lava flow site is counted as a separate unit. Following this counting strategy, since the creation of OVPF (late-1979) until the end of 2019, a period when the volcano has been continuously monitored so that the inventory can be trusted to be 100 % complete, the volcano erupted 77 times within which we can identify 128 distinct lava flows (Table S1). This translates to around 1.7 lava flows per eruption.

Given the fact that lava flows are more frequent in the Enclos than beyond its limit, we had to count the number of  
200 lava flows inside the Enclos based on a different period than for the flows outside of the Enclos. For this, we divided the volcano into five regions: the Enclos, and the *Hors Enclos*, which was sub-divided into northeast flank (NE), southeast flank (SE) and the highlands along the N120 rift zone (N120; Fig. 2a) and the rest. Inside the Enclos, we consider a time period since 1931 (the date since which a rigorous record and mapping has been possible; Derrien, 2019). Until the end of 2019, this involved a total of 195 individual lava flows (Fig. 2a; Table 1; Table S1). The recurrence time of lava flows within the Enclos  
205 is therefore estimated at one every ~5.4 months for the 1931-2019 period. Over this period, only three eruptions occurred outside of the Enclos, and six lava flows were counted for these three events (three in 1977, two in 1986 and one in 1998). To calculate the recurrence time of *Hors Enclos* lava flows, six is a rather small number if we are to ensure a good statistical representation. We therefore increased the time period to extend back to 1708. Over the 1708–2019 period, fifteen lava flows were registered outside the Enclos (Fig. 2b; Table 1; Table S1). Nine lava flows occurred on the southeast flank of the volcano.  
210 Of these, five were observed (in 1774, 1776, 1800 and two in 1986). A sixth event was dated at  $80 \pm 35$  BP using  $C^{14}$  dating on the carbon in the soil below the Piton Raymond lava flow (Vergniolle and Bachèlery, 1982), and three others were dated at 1726, 1765 and 1823 by measuring the base diameter of pioneer trees (Albert et al., 2020). Five other flows were observed on the northeast flank (one in 1708, three in 1977 and one in 1998). Within the less active N120 rift zone, the number of historical eruptions is not large. According to Morandi et al., (2016), eleven tephra or lava flow deposits can be dated since  $2920 \pm 30$  BP,  
215 but only one lava flow has been dated after 1708 (Fig. 2b; Table 1; Table S1). This eruption (named Piton Rampe 14) was dated by  $C^{14}$  at  $140 \pm 90$  BP (Vergniolle and Bachèlery, 1982; Morandi et al., 2016). However, this eruption was not observed and has not been further studied. Another recent eruption is also suggested from some poorly characterized deposits (lapilli) close to the Trous Blancs area at  $145 \pm 30$  BP (Morandi et al., 2016), but no lava flow has been identified associated with this event. However, if we consider only one lava flow since  $140 \pm 90$  BP, or the eleven eruptions since  $2920 \pm 30$  BP, the eruption  
220 recurrence time does not vary significantly (one every 263 years and 209 years for the two periods, respectively). We therefore assume just one eruption over our 311 year period of records for the N120 rift zone.

Overall, the inventory of Table S1 represents a minimum bound on eruptive activity because it is possible that other eruptions and lava flows were not observed nor have yet been identified in the geological record or dated. The minimum recurrence of *Hors Enclos* lava flows since 1708 is therefore estimated at one every ~21 years (Table 1). The relative  
225 occurrence probability is thus calculated by normalizing the number of lava flows per year within each region over the given period. The resulting relative probability of occurrence for a lava flow is 97.99 % inside the Enclos and 2.01 % outside of the



Enclos. Beyond the Enclos relative probability can be divided into 1.29, 0.67 and 0.20 % for the southeast, northeast and N120 rift zones, respectively (Table 1).

#### 4 Probability of vent opening

230 DOWNFLOW has been previously applied to produce lava flow hazard maps at Mount Etna (Favalli et al., 2009c, 2011),  
Nyriragongo (Chirico et al., 2009; Favalli et al., 2009b), Mount Cameroon (Favalli et al., 2012), and Fogo (Richter et al., 2016).  
We here follow the same methodology developed since (Favalli et al., 2009c) and assume that future vents are more likely to  
open in areas where previous vents cluster. The probability of future vent opening is therefore determined on the basis of  
location of historical vents and scaled to the lava flow recurrence probability within each region (cf. sect. 3), under the general  
235 assumption that the characteristics of future eruptions will be similar to those of past eruptions.

Our inventory of vents for Piton de la Fournaise is based on the mapped scoria cone distribution (Davoine and Saint-  
Marc, 2016; Michon et al., 2015; Di Muro et al., 2012; Villeneuve and Bachelery, 2006) and is here updated with all new vents  
formed between 2015 and the end of 2019 (Fig. 3a). Finally, any vents that were missing from this data base but were apparent  
from the mapping of Derrien (2019) were added. The vent density distribution (number of vents per unit area) was then  
240 obtained by applying a Gaussian smoothing kernel to the map of vent locations (Bowman and Azzalini, 2003; Favalli et al.,  
2012; Richter et al., 2016), with a bandwidth that is a function of the local vent density. Within the Enclos, the highest  
concentration is located to the southeast of the summit crater and is up to 51 vents per km<sup>2</sup>. To the east, the concentration  
decreases from 8 vents per km<sup>2</sup> in the Enclos Fouqué caldera, to 3 and 0.5 vents per km<sup>2</sup> in the Grandes Pentés, and the Grand-  
Brûlé, respectively. Outside of the Enclos, resulting vent densities range from 0.01 to 8 vents per km<sup>2</sup> in the rift zones, with a  
245 highest concentration of up to 21 vents per km<sup>2</sup> within the PRVA (as already noted by Michon et al., 2015).

We find that, of the 726 mapped vents, 45 % (327) are within the Enclos, while 55 % (399) are outside of the Enclos.  
For the Hors Enclos vents, 19.6 % (142) are on the N120 rift zone, 13.5 % (98) are on the southeast flank, 6.7 % (49) are on  
the northeast flank, and 15.1 % (110) are elsewhere on the volcano flanks (Table 2). These distributions of vents per region  
differ significantly from the lava flow relative occurrence probability per region (Table 1). For example, while the N120 rift  
250 zone accounts for 19.6 % of the total number of vents (Table 2), only 0.2 % of the lava flows recorded since 1708 have occurred  
in this region (Table 1). Instead, within the Enclos, where ~98 % of the lava flows have been emplaced (Table 1), we count  
only 45 % of the total number of vents (Table 2). This difference is mainly due to the period of time required for cones located  
in the various regions to disappear. In the Enclos, resurfacing processes and landscape changes, such as fissure opening,  
building of new scoria cones over old ones and burial by lava flows occurs at much higher rates than beyond the Enclos.  
255 Therefore, the lifespan of scoria cones (vents) within the Enclos is considerably shorter than compared to that of scoria cones  
outside of the caldera, where 65.8 % of the Enclos has been resurfaced at least once since 1931. Moreover, the selected time  
period (1708-2019) does not cover the full variability in eruption location and activity cycles documented by geological studies  
(Morandi et al., 2016 and references therein), where (in the geologic past) eruptions outside of the Enclos have, at times, been



much more frequent than during the last 300 years. For this reason, the sum of probability density function for future vent opening within a given region of the volcano was set equal to the relative occurrence probability of lava flow in that region. The resulting map of the probability density function of vent opening per unit area is given in Figure 3b. The highest probabilities exceed 10 %/km<sup>2</sup> with a maximum of 24 %/km<sup>2</sup> at the summit crater and across the proximal area of the terminal shield, while moderate values are obtained across the Grandes Pentes and in the Grand-Brûlé (0.01–0.5 %/km<sup>2</sup> and 0.003–0.01 %/km<sup>2</sup>, respectively, Fig. 3b). The northeast and southeast rift zones also have low to moderate values (0.5–0.003 %/km<sup>2</sup>), while the N120 rift zone has a value of less than 0.003 %/km<sup>2</sup>. For the rest of the volcano the probability of vent opening is very low, being less than 0.0001 %/km<sup>2</sup>. However, we note an area of relatively high values (up to 0.5 %/km<sup>2</sup>) located at the PRVA (Fig. 3b).

## 5 DONWFLOW model calibration

Lava flows are gravitational flows that follow the steepest descent path defined by the underlying topography (Harris, 2013). DOWNFLOW is a numerical code that computes the steepest descent paths while randomly applying a given vertical perturbation ( $\Delta h$ ) at every pixel of the DEM (Favalli et al., 2005). By iteration over a thousands of runs ( $N$ ), the code computes all the possible flow paths from the vent to the edge of the DEM through introducing random noise (with a value of  $\pm \Delta h$ ) into each run, so as to produce a probabilistic estimation of the lava flow inundation area. Thus, before applying DOWNFLOW to a given case, the key input parameters  $\Delta h$  and  $N$  need to be defined for the volcano and DEM in question (e.g., Favalli et al., 2012; Richter et al., 2016). Calibrating DOWNFLOW therefore consists of finding the parameters  $\Delta h$  and  $N$  that are able to best fit the model-generated and actual lava flow areas (Favalli et al., 2005). To do this at Piton de la Fournaise, a range of  $\Delta h$  (0 to 5 m) and  $N$  (100 to 10000) were applied to the first lava flows that occurred immediately after the date of DEM generation. DOWNFLOW then computes the array of steepest descent paths out to the limit of the DEM, which, in our case, is the coast, but does not allow computation of lava flow lengths. Therefore, for the calibration, the simulations were cut at actual the length of the flow under consideration (Fig. 4). Following Favalli et al., (2009b) and Richter et al. (2016), the best fit parameters can be found by comparing the actual, mapped, lava flow area ( $A_R$ ) with that generated by the DOWNFLOW simulation ( $A_S$ ):

$$\mu = \frac{A_S \cap A_R}{A_S \cup A_R}, \quad (1)$$

If this ratio ( $\mu$ ) is one then the two areas coincide perfectly and the simulation is valid. However, as the ratio trends towards zero the simulation becomes increasingly unrealistic.

We performed three calibrations, one for each of the three available DEMs (Figure 4). In total, we ran 70,000 simulations and found that input parameters are slightly different for each DEM. For the calibration based on the 1997 DEM, five flows from 1998 to 2007 were considered and we obtained a best fit of  $\mu = 0.50$  for  $N > 6000$  and  $\Delta h > 4$  m. For the calibration based on the 2010 and 2016 DEMs, we considered four and six flows between 2010–2015 and 2016–2019,



290 respectively. The best fit was  $\mu = 0.54$  and  $\mu = 0.51$ , respectively, for  $N > 5000$  and  $\Delta h$  of around 2 m (Fig. 4). The calibration parameters chosen to run DOWNFLOW and build the hazard maps were  $N = 10,000$  for all DEMs and  $\Delta h = 5$  m for the 1997 DEM and  $\Delta h = 2$  m on both the 2010 and 2016 DEMs.

## 6 Lava flow length

To properly evaluate the probability of lava flow inundation, an estimate of expected lava flow lengths is required. Several methods exist to estimate the most likely length of a lava flow. For example, at Etna Favalli et al. (2005) observed a linear relationship between the altitude of the main vent and the maximum possible length of the associated flow. Another method is based on the empirical relationship between the average effusion rate during an eruption and the length of the flow (Walker, 1973). Alternatively, expected cooling-limited flow lengths can be calculated using a thermo-rheological model, such as FLOWGO (Harris and Rowland, 2001), that use theoretical flow cooling and crystallization properties to estimate the point at which forward motion is no longer rheologically possible (Rowland et al., 2004; Wright et al., 2005). Here, at Piton de la Fournaise no clear relationship was found between lava flow length and vent elevation. Due to the great changes in slope within the Enclos ( $<3^\circ$  in the Enclos Fouqué to  $35^\circ$  in the Grandes Pentes area), and the presence of deep valleys on the volcano flanks, no clear relation was found between effusion rate and lava flow run out as calculated with the FLOWGO model. Given the high number of lava flows, it is instead possible to compute a function that represents the lava flow length frequency distribution. To generate this we measured the length of all lava flows emplaced within the Enclos since 1931, and produced functions relevant for each DEM, i.e., until 1997, 2010 and 2016, as well as until the end of 2019 (Fig. 5). For the *Hors Enclos* lava flows, we extended the database to all flow units that have been mapped by Bachèlery and Chevallier (1982), even if they are not dated, which gave us a total of 43 lava flows to work with (see also Di Muro et al., 2012; Principe et al., 2016; Fig. 5, Fig. S1).

## 310 7 Probabilistic lava flow hazard maps

To produce the hazard map for each DEM, a 100-m spaced grid of computational vents was defined for the whole of Piton de la Fournaise and a total of 126,000 simulations, of which 12,000 were inside the Enclos, were run using DOWNFLOW. From this database of simulations, it was possible to construct the lava flow hazard map which gives the probability, at each point, of inundation by lava flow upon the occurrence of the next effusive eruption (Rowland et al., 2005; Wright et al., 2008). The hazard at any pixel  $i$  is thus defined as the probability  $H_i$  that the pixel will be inundated by a lava flow, and is given by (Favalli et al., 2012):

$$H_i = \sum_j \rho_{Vj} \Delta x \Delta y \cdot P_{ij} \cdot P_{Lij} , \quad (2)$$



where the sum extends over all possible vent locations  $j$  with the coordinates  $x_j$  and  $y_j$ ,  $\Delta x$  and  $\Delta y$  define the pixel size and  $\rho_{Vj}$  is the probability density function of vent opening at location  $j$  (this is shown for the whole edifice in Fig. 3b). The mask of the simulations obtained with DOWNFLOW is given by  $P_{ij}$ , where pixel  $i$  has the value one if inundated by a lava flow originating from vent location  $j$  and has a value of zero otherwise (irrespective of the distance between  $j$  and  $i$ ). Finally,  $P_{Lij}$  is the probability that a lava flow originating from vent  $j$  reaches pixel  $i$  along the calculated flow path, and is obtained by converting the frequency distribution of lava flow length for all flows up to relevant date (Fig. 5) into a probability.

### 7.1 Hazard map for the entire volcano

To be as up-to-date as possible, the hazard map for the entire volcano was derived using a combination of the 2016 DEM for the Enclos area and the 2010 DEM for the rest of the volcano (Fig. 6). We can do this, because the 2010 DEM will not have been affected by topographic change outside of the Enclos. We run DONWFLOW using the best fit parameters as determined for the 2010-2019 period (Fig. 4c). In the Enclos, the lava flow length distribution was determined over 1931-2019, while for rest of the volcano, we considered the length of the flow units mapped by Bachèlery and Chevallier (1982) (cf. Sect. 7; Fig. 5, Fig. S1). This is then convolved with the probability density function of vent opening from all the historical vents presented in Figure 3b following Equation 2 (cf. Sect. 5).

#### *Inside the Enclos*

The resulting map (Fig.6) clearly shows that the highest probability of lava flow inundation at Piton de la Fournaise is located within the Enclos, where 47 % of the Enclos has a high (>1 %) probability of lava inundation. Within the summit crater, in some places of the Enclos Fouqué and across parts of the Grandes Pentès, the probability is extremely high (>10 %). In the Grand-Brûlé area the probability is intermediate (up to 2 %) to low (0.1–0.5 %) due to the low probability of vent opening as well as the relative short lava flow length distribution (in the Enclos only 11 lava flows have reached the ocean since 1931). We note that there is a relatively high probability (of up to 2 %) that the flows will cut the belt road in some places.

#### *Outside the Enclos*

The highest probability of lava flow inundation outside of the Enclos is up to 0.5 % and is on the southeast and northeast flanks of the volcano as well as in the PRVA (Fig. 6). The less active N120 rift zone has a very low, but still non-negligible, probability of lava flow invasion (<0.01 %). Although the probability of vent opening is higher at greater altitudes (Fig. 3), the lava flow length is usually longer outside of the Enclos than it is inside (Fig. 5). This implies that the probability of lava flow inundation remains the same as distance increases from the vent. This means that outside of the Enclos the distribution of the probability of lava flow inundation seems to depend mostly on the preferential flow path rather than the distance from the vent.



## 7.2 Evolution of hazard maps with DEM within the Enclos

Given the very high number of eruptions and the existence of three DEMs, we can compare the evolution of the lava flow hazard distribution within the Enclos with time and construction of new topography (Fig. 7). To do this we built three hazard maps, one for each of the DEMs. That is, in 1997, 2010 and 2016. For each map, we take the appropriate lava flow length distribution, relative recurrence time and vent distribution from time of DEM generation back to 1931 (Fig. 5; Table 3), with the DOWNFLOW calibration tailored to each case (Fig. 4). The percentage of vents in the summit craters versus those forming in the rest of the Enclos is roughly the same at the end of 2019 as in 1997 (that is around 3.4–6.1 % of the vents are within the crater, Table 3). This is important, because lava emitted from a vent opening in the summit crater will become entrapped in the pit, and will not be free to flow down slopes of the Enclos. The results also show that since 1931 the number of vents opening increased from 88 between 1931 and 2010, to 186 between 1931 and 2019 (Table 3). The number of lava flows emitted also increased from 106 for the period 1931–1997, to 200 for the period 1931–2019. Instead, the relative probability of lava flow in the summit craters decreased from 27.9 % in 1997 to 24.1 % in 2019, reflecting that eruptions within the craters become rarer over the analyzed period, becoming non-existent since 2014.

The three hazard maps for the Enclos (Fig. 7) show that the highest probabilities (2 to >10 %) of lava flow inundation are concentrated in the Enclos Fouqué area (above 1800 m a.s.l.). Between the 1997 and 2010, we note the development of a high probability area to the north of the terminal shield, and a slight decrease in probabilities to the southeast. This is due to the high number of eruptions occurring to the north of the shield between 1998 and 2006 (see Fig. S2). On the 2016 hazard map, the southeast part of the Enlos Fouqué shows a smaller high probability area, but with higher values of up to 12 %. This reflects a focusing of vent opening in this area over the period 2010–2016. Figure 7 also illustrates that the hazard maps were able to predict where subsequent lava flows actually occurred. Lava flows subsequent to each map were all emplaced in high probability areas, and most of the flows did not extend onto the moderate (5 %) probability zone. The exception is the 2007 eruption that occurred at a low altitude in the Grand-Brûlé, and which represents the largest eruption of the considered period. This is the only event to have occurred in a low (<1 %;) probability zone (Fig. 7).

## 8 Discussion

### 8.1 Hazard map interpretation

According to Calder et al. (2015), uncertainties in hazard maps are mainly related to three issues. These are (Calder et al., 2015):

“(i) the incompleteness and bias of the geological record and the extent to which it represents possible future outcomes; (ii) the fact that analyses based on empirical models rely on a priori knowledge of the events; and (iii) the ability of complex computational models to adequately represent the full complexity of the natural phenomena”.



Our hazard maps presented here in Figures 6 and 7 have been produced from available historical and geological records of when and where past lava inundation has occurred at Piton de la Fournaise, as well as vent location, lava flow location, recurrence, and length. The quality and detail of these records improve with time, and are better inside the Enclos than outside. Secondly, the maps are based on stochastic simulations of lava flow paths, the reliability of which depend on the quality, and up-to-dateness of our topographic model (DEM). This is an issue at a frequently active effusive center, where emplacement of new lava units causes the topography to be in a state of near-constant change. Here we thus discuss the uncertainties related to the interpretation of the presented maps and the extent to which they are adequate in assessing risk associated with future eruptions.

### 8.1.1. Historical and geological records: representativeness of future eruptions

Our geographical distribution of vent density per unit area (Fig. 3b) is based on an inventory of 726 vents and includes pre-historic vents (scoria cones) identified in the geological record back to at least 57 ka BP (McDougall, 1971). The lava flow inventory and recurrence probability inside the Enclos covers a time span of 88 years (from 1931 to 2019), and outside the Enclos the record spans 311 years (from 1708 to 2019). Given the frequency of activity, this allows a comprehensive data set of 220 lava flows to be used (Table S1). These relatively long periods and large numbers of cases, mean that the hazards maps produced here provide the future vent opening and lava flow inundation probabilities relevant at a temporal scale spanning decades to centuries, and are based on a statistically robust data set. They should therefore be reliable and trustworthy for long term land use planning and management. This includes agricultural practices, urban planning, road network planning, assignment of protected areas, park-use planning, implementation of trail networks and installation of subterranean and above ground electric, sewage and gas networks; as well as targeting of potential zones where repair and replacement will be necessary (e.g. Tsang et al., 2020). Nonetheless, although, we argue that this hazard map is trustworthy in the long term, it may not be adapted for the short term, i.e., the next few years, over small spatial scales, i.e., hundreds of meters. Given the frequent resurfacing of the Enclos, the topography of the Enclos is highly variable in the short term, where emplacement of new lava flow units can cause subsequent flows to advance down paths that are displaced 10s to 100s of meters over what would have been the case had the initial, pre-eruption, topography applied (Harris and Rowland, 2015). As shown in Harris et al. (2019), emplacement of new flow units, locally, can invalidate a DEM in a matter of hours, causing subsequent flow paths impossible to replicate. Thus, to accurately and precisely forecast exact lava flow paths the topography needs to be revised after each eruption, and even during long-lasting (weeks-to-months long) eruptions. As shown in Figure 6, the lava flow inundation probability distribution changes over the time span of a few years. However, although precise hazard maps for such active centers need to be regularly updated, over the time span of decades to centuries, the topography remains broadly the same, where in the case considered here the Enclos has a slope profile that is downhill from east to west, guiding flow towards the coast (Fig. 6).

The interpretation of the hazard map may also need to vary with time as a system cycles through phases of more and less frequent activity, and as the intensity of events within each cycle wax and wane. Activity at Piton de la Fournaise follows



cycles that evolve over time scales of a few years to a decade or so (Derrien, 2019; Got et al., 2013; Peltier et al., 2009; Roullet et al., 2012; Vlastélic et al., 2018). This cyclic eruptive pattern will control the location, intensity and magnitude of the eruptions, and hence the location, length and area of inundation of associated lava flows. Eruptive fissures tend to be closer to the summit craters (i.e., proximal eruptions are more probable) at the start of a cycle than at the end (when distal eruptions are more likely to occur). Moreover, cycle durations will depend on the magma supply rate, where the lower the supply rate the longer the cycle (Derrien, 2019). Cycles also often terminate with a relatively long-lived, high volume, and high intensity effusive event (Coppola et al., 2017). Therefore, depending on the length of cycle and where, temporally, in the cycle we are, both the geographical distribution of the probability of vent opening and the length of associated flow will vary.

Piton de la Fournaise also experiences longer-duration (20-30 year long) cycles that are related to systematic evolution in the fertility of the magma source (Vlastélic et al., 2018). Phases of increasing mantle fertility are related to increasing eruption frequency and erupted volume, as the mantle porosity increases thus promoting melt extraction. Such increasing phases of activity ultimately culminate in exceptionally voluminous, eruptions with high effusion rates, as well as summit collapse or pit-crater formation; as occurred in 1931, 1961, 1986 and 2007 (Vlastélic et al., 2018). Given that the lava flow length will be related to effusion rate and lava volume (Harris and Rowland, 2001; Malin, 1980; Pinkerton and Wilson, 1994; Walker, 1973), the lava length frequency distribution used to compute the hazard map is thus dependent on where, in terms of time, we are in such a longer-term source-related cycle. In addition, the collapse and pit crater formation events at the end of the cycle will strongly modify the topography in the proximal region.

Because our hazard maps are based on a database whose events are dominated by “typical” eruptions (i.e., only four or the 137 eruptions since 1931 are high volume source-related-cycle terminating events), they are representative only of such typical cases and event scenarios. Therefore, the maps cannot be applied to assess the hazard associated with such “atypical” (source-related-cycle terminating) events. To illustrate this point, we take the 1997 hazard map (Fig. 7a). In this map, the 2007 lava flow is not well predicted where it occurred in a low (<0.5 %) probability zone. For the reasons mentioned above, the occurrence of atypical eruptions (such as the 1931, 1961, 1986 and 2007 events) cannot thus be foreseen by this particular set of hazard maps. This is a major issue in terms of risk because such atypical events have exceptionally high lava discharge rates (which were sustained at more than 100 m<sup>3</sup>/s over 30 days in 2007; Staudacher et al., 2009), with flows advancing rapidly (within hours of the eruption onset) cut the belt road and enter the ocean (Harris and Villeneuve, 2018a). As a result, they are capable of rapidly inundating large areas to cause extensive damage. They thus represent the highest risk effusive event at Piton de la Fournaise, but are not accounted for in our hazard maps. Dedicated studies on the probability of occurrence of such high magnitude and intensity, but atypical, events needs to be conducted, and a separate set of hazard maps are required for such events. Likewise, our analysis does not consider the poorly studied, but relatively recent (post-1708), long-lasting activity related to overflow from summit lava lakes, as was common between 1750 - 1800 and around 1850 (Michon et al., 2013; Peltier et al., 2012). Our maps are, though, applicable to the most commonly effusive event scenario currently encountered at Piton de la Fournaise. However, they must be used and trusted with the above caveats in mind regarding the type of activity and effusive event to which they apply.



### 8.1.2. Numerical modelling

The DOWNFLOW stochastic approach computes the lava flow inundation area by summing  $N$  lava flow paths for a given random vertical perturbation ( $\Delta h$ ) added to the DEM. As discussed above, the DEM thus needs to be regularly updated when a high frequency of lava flow emplacement events modifies the topography. The DOWNFLOW calibration requires a choice of two main parameters: the number of runs and the maximum range of  $\Delta h$ . The parameter space of Figure 4 shows that the required number of runs ( $N$ ) needed to achieve a good fit with the lava flow area ( $\mu > 0.5$ ) must, in this case, be at-least 2 000–5 000. Therefore, a safe choice for  $N$  to ensure statistically robust simulations is 10 000 in all cases, and this is used here to ensure model (and output map) robustness (Tarquini and Favalli, 2013). The calibration for  $\Delta h$  gives different results for pre- and post-2007 cases, being 5 m and 2 m, respectively. According to Favalli et al. (2005),  $2\Delta h$  represents the characteristic vertical height of an obstacle that the flow can overcome. This implies that, since 2007, lava flow dimensions have changed: they must have become thinner as they can now only overflow an obstacle if that obstacle is 3 m lower than prior to 2007. Indeed, the lava flows in our data base are more voluminous, longer and thicker between 1997 and 2007 (mean length: 6480 m, mean volume:  $49 \times 10^6 \text{ m}^3$ , mean thickness 12.5 m) than between 2007 and 2019 (mean length: 2500 m, mean volume:  $3.5 \times 10^6 \text{ m}^3$ , mean thickness 4.3 m). This difference can be related to the cyclic activity. The period between 1997 and 2007 corresponds to end of a deep source cycle (Cycle 3 of Vlastélic et al., 2018). As a result, lavas were increasingly associated with higher magma fertility and magma supply rates, to produce more voluminous flows at relatively high effusion rates. Hence, following Walker (1973) and Malin (1980) units were longer and thicker, and thus able to overcome higher obstacles. However, the period after 2007 relates to the beginning of a new deep source cycle (Cycle 4 of Vlastélic et al., 2018), with lower fertility and output rates. During this period the reverse is true: flows were less voluminous, and hence shorter and thinner and able to only overcome lower obstacles. The calibration parameters used for DOWNFLOW, especially  $\Delta h$ , thus must be determined for, and then applied to, a specific period of activity if the results are to be valid; and changed should there be an evolution in a cycle or eruption style.

### 8.2 Use for hazard mitigation at Piton de la Fournaise

In terms of hazard mitigation at Piton de la Fournaise, our maps are intended to provide information of value in planning actions implemented by local authorities and in building resilience to future eruptions, with a focus on protection of public infrastructure. Figure 6 shows the locations of all roads and hiking trails that are the most likely to be covered by future lava flows, and the lengths of each that may need to be replaced.

For the island belt road, we see that 4.5 km of the 10 km that crosses the Enclos is in an intermediate probability ( $>0.5$  %, Fig. 6) zone in terms of lava inundation. We also see that even if the probability is low, the probability of lava flow invasion is not negligible for several municipalities situated beyond the Enclos on the northeast and southeast flanks of the volcano (i.e., Saint-Phillipe and Sainte-Rose, Fig. 6). In terms of hiking trails, although the main trail to the summit crater is in a low probability zone in terms of lava inundation, it is in a very high probability zone in terms of vent opening ( $>2 \text{ %/km}^2$ , Fig. 3).



Regularly since 2014, trails inside the Enclos Fouqué have been covered by lava, as for example in February 2019 when 400 m of trail very close to the viewing platform for the summit crater was buried (OVPF reports, ISSN 2610-5101).

480 In the case of an imminent eruption, our hazard map will thus complement the real time information that OVPF shares with civil protection, who need to identify potential locations from where people may need to be evacuated and road sections to be closed (Peltier et al., 2020). In addition, land use plans (referred as *Plan de Prévention des Risques* in French law) at La Réunion do not currently take into account volcanic hazard. Our maps are thus also intended to aid and guide stakeholders in developing effective and comprehensive mitigation and land use plans, with the caveat that our maps are for a “typical” effusive  
485 event. Separate maps will need to be drafted in the future for atypical events, including high intensity events and prolonged lava lake overflow at the summit, and this map should be updated whenever topography changes and a new DEM becomes available. However, we have here provided a flexible methodology that allows for ease of up-date.

## 9 Conclusion

Piton de la Fournaise is one of the most active effusive centers in the world, it being a volcano that has experienced more than  
490 one eruption a year since human settlement of the island at the end of the 17<sup>th</sup> century, and two eruptions a year since the volcano has been closely monitored by OVPF since 1979. The resulting database to calculate lava flow frequency and probability of future vent opening thus comprises 207 individual lava flows emplaced within the Enclos since 1931, 15 lava flows emplaced outside of the Enclos since 1708 and 726 vents over the entire volcano edifice. This large data base allows compilation of a statistically robust hazard assessment and production of probabilistic hazard maps for lava flow inundation.  
495 Within the most active area of the volcano (i.e, the Enclos), a lava flow has been emitted every 5.3 months since 1931, 13 of which have cut the island belt road, while beyond the caldera, an effusive event has occurred on average every 21 years over the last three centuries. Since 1931, two Hors Enclos eruptions since 1977 have caused property damage and twelve lava flows have cut the belt road.

Our lava flow hazard map uses these data, with lava flow path projections based on the stochastic model  
500 DOWNFLOW, to identify those areas that are most likely to be impacted by lava flows during any future eruption, and to quantify the probability of inundation. Fundamentally we stress the need for frequent update of the DEMs at such frequently active volcanoes, where topography is constantly evolving to influence flow path, so as to produce a series of hazard maps that evolve with time and topography. In addition, given that the activity follows cycles that cause the location, erupted lava volume, effusion rate and flow dimensions to evolve with time, both the maps and the parameters used for modelling need to be applied  
505 on a case-dependent basis. We here produce maps that apply to effusive events that typify the first and second phases of a cycle, but not the terminating high-volume events. Dedicated studies for probability occurrence of such high-volume events thus need to be conducted to complete the hazard assessment for all effusive scenarios. Our lava flow hazard map methodology is, though, intended as a flexible approach that can be applied to frequently active effusive centers, producing up-to-date maps



that can be updated as eruption conditions evolve. This is essential support for informed land-use planning, as well as for use  
510 in crisis response and in drafting of hazard mitigation plans.

### Supplementary material

Table S1: Table of the inventory of eruptions and lava flows since 1708

Figure S1: Map of the extracted lava flow length

515 Figure S2: Figure of the lava flows for each period of time (1972-1992; 1998-2007; 2010-2015; 2016-2019)

### Data availability

All data shown in this study including the eruption inventory and GIS layers (georeferenced .shp files of the vents, fissures  
and lava flows as well as the calculated density function of vent opening and hazard maps) are freely available upon request  
520 at the OVPF or in the supplementary material.

### Authors contribution

MOC lead this study, wrote the manuscript and made all figures and tables. MF executed the vent probability distribution, the  
DOWNFLOW calibration and computed the hazard maps; NV wrote the DEM section; AP, ADM and NV contributed to the  
525 eruption inventory; AD and NV draw the lava flow outlines; PB compiled the GIS data. All authors contributed to  
implementing the discussion and to the writing of the article.

### Acknowledgements

This research was fully funded by the Agence National de la Recherche through the project LAVA (Program: DS0902 2016;  
530 Project: ANR-16 CE39-0009, <http://www.agence-nationale-recherche.fr/Projet-ANR-16-CE39-0009>). This is ANR-LAVA  
contribution no. XX and IPGP contribution no. XX.

### References

- Albarède, F., Luais, B., Fitton, G., Semet, M., Kaminski, E., Upton, B. G. J., Bachèlery, P. and Cheminée, J. L.: The  
geochemical regimes of piton de la Fournaise volcano (Réunion) during the last 530000 years, *J. Petrol.*, 38(2), 171–201,  
535 doi:10.1093/etroj/38.2.171, 1997.
- Albert, S., Flores, O., Michon, L. and Strasberg, D.: Dating young (<1000 yrs) lava flow eruptions of Piton de la Fournaise  
volcano from size distribution of long-lived pioneer trees, *J. Volcanol. Geotherm. Res.*, 401(106974),  
doi:10.1016/j.jvolgeores.2020.106974, 2020.
- Arab-Sedze, M., Heggy, E., Bretar, F., Berveiller, D. and Jacquemoud, S.: Quantification of L-band InSAR coherence over  
540 volcanic areas using LiDAR and in situ measurements, *Remote Sens. Environ.*, 152, 202–216, doi:10.1016/j.rse.2014.06.011,



- 2014.
- Bachèlery, P.: Le Piton de la Fournaise (Ile de La Réunion). Etude volcanologique, structural et pétrologique, Univ. Clermont-Ferrand II., 1981.
- Bachèlery, P. and Chevallier, L.: Carte volcano-structurale du massif de la Fournaise au 1/50 000e avec notice explicative, 545 Publ. Inst. Phys. du Globe Paris, 1982.
- Bertile, W.: Des coulées volcaniques à Saint-Philippe (Mars 1986) : gestion d'une catastrophe naturelle, Edition Co., Saint-Denis, La Réunion., 1987.
- Boivin, P. and Bachèlery, P.: Petrology of 1977 to 1998 eruptions of Piton de la Fournaise, La Réunion Island, J. Volcanol. Geotherm. Res., 184(1), 109–125, doi:https://doi.org/10.1016/j.jvolgeores.2009.01.012, 2009.
- 550 Bonne, K., Kervyn, M., Cascone, L., Njome, S., Van Ranst, E., Suh, E., Ayonghe, S., Jacobs, P. and Ernst, G.: A new approach to assess long-term lava flow hazard and risk using GIS and low-cost remote sensing: The case of Mount Cameroon, West Africa, Int. J. Remote Sens., 29(22), 6539–6564, doi:10.1080/01431160802167873, 2008.
- Bowman, A. W. and Azzalini, A.: Computational aspects of nonparametric smoothing with illustrations from the sm library, Comput. Stat. Data Anal., 42(4), 545–560, doi:10.1016/S0167-9473(02)00118-4, 2003.
- 555 Bretar, F., Arab-Sedze, M., Champion, J., Pierrot-Deseilligny, M., Heggy, E. and Jacquemoud, S.: An advanced photogrammetric method to measure surface roughness: Application to volcanic terrains in the Piton de la Fournaise, Reunion Island, Remote Sens. Environ., 135, 1–11, doi:10.1016/j.rse.2013.03.026, 2013.
- Calder, E. S., Wagner, K. and Ogburn, S. E.: Chapter 20 Volcanic hazard maps, in Global Volcanic Hazards and Risk, edited by S. C. Loughlin, R. S. J. Sparks, S. Brown, S. K. Jenkins, and C. Vye-Brown, Cambridge University Press, Cambridge., 560 2015.
- Cappello, A., Zanon, V., Del Negro, C., Ferreira, T. J. L. and Queiroz, M. G. P. S.: Exploring lava-flow hazards at Pico Island, Azores Archipelago (Portugal), Terra Nov., 27(2), 156–161, doi:10.1111/ter.12143, 2015.
- Chirico, G. D., Favalli, M., Papale, P., Boschi, E., Pareschi, M. T. and Mamou-Mani, A.: Lava flow hazard at Nyiragongo Volcano, DRC 2. Hazard reduction in urban areas, Bull. Volcanol., 71(4), 375–387, doi:10.1007/s00445-008-0232-z, 2009.
- 565 Coppola, D., Di Muro, A., Peltier, A., Villeneuve, N., Ferrazzini, V., Favalli, M., Bachèlery, P., Gurioli, L., Harris, A. J. L., Moune, S., Vlastélic, I., Galle, B., Arellano, S. and Aiuppa, A.: Shallow system rejuvenation and magma discharge trends at Piton de la Fournaise volcano (La Réunion Island), Earth Planet. Sci. Lett., 463, 13–24, doi:10.1016/j.epsl.2017.01.024, 2017.
- Davoine, P. and Saint-Marc, C.: A Geographical Information System for Mapping Eruption Risk at Piton de la Fournaise., in Active Volcanoes of the Southwest Indian Ocean. Active Volcanoes of the World., edited by P. Bachèlery, J.-F. Lénat, A. Di 570 Muro, and L. Michon, Springer., 2016.
- Derrien, A.: Apports des techniques photogrammétriques à l'étude du dynamisme des structures volcaniques du piton de la fournaise, Université de Paris., 2019.
- Derrien, A., Villeneuve, N., Peltier, A. and Michon, L.: Multi-temporal airborne structure-from-motion on caldera rim: Hazard, visitor exposure and origins of instabilities at Piton de la Fournaise, Prog. Phys. Geogr. Earth Environ., 43(2), 193–214,



- 575 doi:10.1177/0309133318808201, 2018.
- Derrien, A., Peltier, A., Villeneuve, N. and Staudacher, T.: The 2007 caldera collapse at Piton de la Fournaise: new insights from multi-temporal structure-from-motion, *Volcanica*, 3(1), 55–65, doi:10.30909/vol.03.01.5565, 2020.
- Duffield, W. A., Stieltjes, L. and Varet, J.: Huge landslide blocks in the growth of piton de la fournaise, La réunion, and Kilauea volcano, Hawaii, *J. Volcanol. Geotherm. Res.*, 12(1), 147–160, doi:https://doi.org/10.1016/0377-0273(82)90009-9, 580 1982.
- Dvorak, J., Okamura, A. and Dieterich, J. H.: Analysis of surface deformation data, Kilauea Volcano, Hawaii: October 1966 to September 1970, *J. Geophys. Res. Solid Earth*, 88(B11), 9295–9304, doi:https://doi.org/10.1029/JB088iB11p09295, 1983.
- Favalli, M., Pareschi, M. T., Neri, A. and Isola, I.: Forecasting lava flow paths by a stochastic approach, *Geophys. Res. Lett.*, 32(3), 1–4, doi:10.1029/2004GL021718, 2005.
- 585 Favalli, M., Tarquini, S., Fomaciaci, A. and Boschi, E.: A new approach to risk assessment of lava flow at Mount Etna, *Geology*, 37(12), 1111–1114, doi:10.1130/G30187A.1, 2009a.
- Favalli, M., Chirico, G. D., Papale, P., Pareschi, M. T. and Boschi, E.: Lava flow hazard at Nyiragongo volcano, D.R.C. 1. Model calibration and hazard mapping, *Bull. Volcanol.*, 71(4), 363–374, doi:10.1007/s00445-008-0233-y, 2009b.
- Favalli, M., Mazzarini, F., Pareschi, M. T. and Boschi, E.: Topographic control on lava flow paths at Mount Etna, Italy: 590 Implications for hazard assessment, *J. Geophys. Res. Earth Surf.*, 114(1), 1–13, doi:10.1029/2007JF000918, 2009c.
- Favalli, M., Tarquini, S. and Fornaciari, A.: Downflow code and lidar technology for lava flow analysis and hazard assessment at mount etna, *Ann. Geophys.*, 54(5), 552–566, doi:10.4401/ag-5339, 2011.
- Favalli, M., Tarquini, S., Papale, P., Fornaciari, A. and Boschi, E.: Lava flow hazard and risk at Mt. Cameroon volcano, *Bull. Volcanol.*, 74(2), 423–439, doi:10.1007/s00445-011-0540-6, 2012.
- 595 Felpeto, A., Araña, V., Ortiz, R., Astiz, M. and García, A.: Assessment and modelling of lava flow hazard on Lanzarote (Canary Islands), *Nat. Hazards*, 23(2–3), 247–257, doi:10.1023/A:1011112330766, 2001.
- de Franchis, C., Meinhardt-Llopis, E., Michel, J., Morel, J.-M. and Facciolo, G.: An automatic and modular stereo pipeline for pushbroom images, *ISPRS Ann. Photogramm. Remote Sens. Spat. Inf. Sci.*, II-3, 49–56, doi:10.5194/isprsannals-II-3-49-2014, 2014.
- 600 Gillot, P.-Y., Lefèvre, J.-C. and Nativel, P.-E.: Model for the structural evolution of the volcanoes of Réunion Island, *Earth Planet. Sci. Lett.*, 122(3), 291–302, doi:10.1016/0012-821X(94)90003-5, 1994.
- Got, J. L., Peltier, A., Staudacher, T., Kowalski, P. and Boissier, P.: Edifice strength and magma transfer modulation at Piton de la Fournaise volcano, *J. Geophys. Res. Solid Earth*, 118(9), 5040–5057, doi:10.1002/jgrb.50350, 2013.
- Harris, A.: *Thermal Remote Sensing of Active Volcanoes: A User’s Manual*, Cambridge University Press, Cambridge., 2013.
- 605 Harris, A. J. L. and Rowland, S. K.: FLOWGO: a kinematic thermo-rheological model for lava flowing in a channel, *Bull. Volcanol.*, 63, 20–44, doi:10.1007/s004450000120, 2001.
- Harris, A. J. L. and Rowland, S. K.: Effusion Rate Controls on Lava Flow Length and the Role of Heat Loss: A Review, *Leg. Georg. P.L. Walker, Spec. Publ. IAVCEI. Eds Hoskuldsson A, Thordarson T, Larsen G, Self S, Rowl. S. Geol. Soc. London.*,



- 2, 33–51, 2009.
- 610 Harris, A. J. L. and Rowland, S. K.: Lava flows and rheology, *Encycl. Volcanoes*, 2nd Ed. Eds Sigurdsson H, Hought. B, McNutt SR, Rymer H, Styx J, 2015.
- Harris, A. J. L. and Villeneuve, N.: Newspaper reporting of the April 2007 eruption of Piton de la Fournaise, part 2: framing the hazard, *J. Appl. Volcanol.*, 7, 2018a.
- Harris, A. J. L. and Villeneuve, N.: Newspaper reporting of the April 2007 eruption of Piton de la Fournaise part 1: useful  
615 information or tabloid sensationalism?, *J. Appl. Volcanol.*, 7(1), 4, doi:10.1186/s13617-018-0073-1, 2018b.
- Harris, A. J. L., Chevrel, M. O., Coppola, D., Ramsey, M. S., Hrysiewicz, A., Thivet, S., Villeneuve, N., Favalli, M., Peltier, A., Kowalski, P., DiMuro, A., Froger, J.-L. and Gurioli, L.: Validation of an integrated satellite-data-driven response to an effusive crisis: the April–May 2018 eruption of Piton de la Fournaise., *Ann. Geophys.*, 61, doi:10.4401/ag-7972, 2019.
- Keszthelyi, L. and Self, S.: Some physical requirements for the emplacement of long basaltic lava flows, *J. Geophys. Res.*,  
620 B11, 27,447-27,464, 1998.
- Kieffer, G., Tricot, B. and Vincent, P. M.: Une éruption inhabituelle (avril 1977) du Piton de la Fournaise (Ile de la Réunion) : ses enseignement volcanologiques et structuraux, *Compte Rendu l'Academis des Sci. Paris*, 285, 957–960, 1977.
- Kolzenburg, S., Giordano, D., Di Muro, A. and Dingwell, D. B.: Equilibrium Viscosity and Disequilibrium Rheology of a high Magnesium Basalt from Piton De La Fournaise volcano ,La Réunion, Indian Ocean, France, *Ann. Geophys.*, doi:10.4401/ag-  
625 7839, 2018.
- Lénat, J.-F., Bachèlery, P. and Merle, O.: Anatomy of Piton de la Fournaise volcano (La Réunion, Indian Ocean), *Bull. Volcanol.*, 74(9), 1945–1961, doi:10.1007/s00445-012-0640-y, 2012.
- Lormand, C., Harris, A. J. L., Chevrel, M. O., Calvari, S., Gurioli, L., Favalli, M., Fornaciai, A. and Nannipieri, L.: The 1974 west flank eruption of Mount Etna: A data-driven model for a low elevation effusive event, *Front. Earth Sci.*, xx,  
630 doi:10.3389/feart.2020.590411, 2020.
- Malin, M. C.: Lengths of Hawaiian lava flows, *Geology*, 8(July), 306–308, 1980.
- McDougall, I.: The geochronology and evolution of the young volcanic island of Réunion, Indian Ocean, *Geochim. Cosmochim. Acta*, 35(3), 261–288, doi:https://doi.org/10.1016/0016-7037(71)90037-8, 1971.
- Merle, O. and Lénat, J.-F.: Hybrid collapse mechanism at Piton de la Fournaise volcano, Reunion Island, Indian Ocean, *J.*  
635 *Geophys. Res. Solid Earth*, 108(B3), 1–11, doi:10.1029/2002jb002014, 2003.
- Merle, O., Mairine, P., Michon, L., Bachèlery, P. and Smietana, M.: Calderas, landslides and paleo-canyons on Piton de la Fournaise volcano (La Réunion Island, Indian Ocean), *J. Volcanol. Geotherm. Res.*, 189(1), 131–142, doi:10.1016/j.jvolgeores.2009.11.001, 2010.
- Michon, L. and Saint-Ange, F.: Morphology of Piton de la Fournaise basaltic shield volcano (La Réunion Island):  
640 Characterization and implication in the volcano evolution, *J. Geophys. Res. Solid Earth*, 113(3), 1–19, doi:10.1029/2005JB004118, 2008.
- Michon, L., Cayol, V., Letourneur, L., Peltier, A., Villeneuve, N. and Staudacher, T.: Edifice growth, deformation and rift



- zone development in basaltic setting: Insights from Piton de la Fournaise shield volcano (Réunion Island), *J. Volcanol. Geotherm. Res.*, 184(1), 14–30, doi:10.1016/j.jvolgeores.2008.11.002, 2009.
- 645 Michon, L., DiMuro, A., Villeneuve, N., Saint-Marc, C., Fadda, P. and Manta, F.: Explosive activity of the summit cone of Piton de la Fournaise volcano (La Réunion island): A historical and geological review, *J. Volcanol. Geotherm. Res.*, 264, 117–133, doi:10.1016/j.jvolgeores.2013.06.012, 2013.
- Michon, L., Ferrazzini, V., Di Muro, A., Villeneuve, N. and Famin, V.: Rift zones and magma plumbing system of Piton de la Fournaise volcano: How do they differ from Hawaii and Etna?, *J. Volcanol. Geotherm. Res.*, 303, 112–129,
- 650 doi:10.1016/j.jvolgeores.2015.07.031, 2015.
- Morandi, A., Muro, A. Di, Principe, C., Leroi, G., Michon, L., Morandi, A., Muro, A. Di, Principe, C., Leroi, G., Michon, L., Id, H. A. L., Morandi, A., Muro, A. Di, Principe, C., Michon, L., Leroi, G., Norelli, F. and Bachèlery, P.: Pre-historic (< 5 kiloyear) Explosive Activity at Piton de la Fournaise Volcano, in *Active Volcanoes of the Southwest Indian Ocean*, edited by P. Bachelery, J.-F. Lenat, A. Di Muro, and L. Michon, pp. 107–138, Springer Berlin Heidelberg, Berlin Heidelberg, 2016.
- 655 Morin, J.: Gestion institutionnelle et réponses des populations face aux crises volcaniques : études de cas à La Réunion et en Grande Comore, Université de la Réunion. [online] Available from: <https://tel.archives-ouvertes.fr/tel-01199868>, 2012.
- Mossoux, S., Kervyn, M. and Canters, F.: Assessing the impact of road segment obstruction on accessibility of critical services in case of a hazard, *Nat. Hazards Earth Syst. Sci.*, 19, 1251–1263, doi:10.5194/nhess-19-1251-2019, 2019.
- Di Muro, A., Bachèlery, P., Boissier, P., Davoine, P., Fadda, P., Favalli, M., Ferrazzini, V., Finizola, A., Leroi, G., Levieux,
- 660 G., Mairine, P., Manta, F., Michon, L., Morandi, R., Nave, R., Peltier, A., Principe, C., Ricci, T., Roult, G., Saint-Marc, C., Staudacher, T. and Villeneuve, N.: Evaluation de l'aléa volcanique à La Réunion. [online] Available from: [http://www.reunion.developpement-durable.gouv.fr/IMG/pdf/Rapport\\_1erephase\\_etude\\_volcan\\_web\\_cle534456.pdf](http://www.reunion.developpement-durable.gouv.fr/IMG/pdf/Rapport_1erephase_etude_volcan_web_cle534456.pdf), 2012.
- Di Muro, A., Métrich, N., Vergani, D., Rosi, M., Armienti, P., Fougèroux, T., Deloule, E., Arienzo, I. and Civetta, L.: The shallow plumbing system of Piton de la Fournaise Volcano (La Réunion Island, Indian Ocean) revealed by the major 2007
- 665 caldera-forming eruption, *J. Petrol.*, 55(7), 1287–1315, doi:10.1093/petrology/egu025, 2014.
- Nave, R., Ricci, T. and Pacilli, M. G.: Perception of Risk for Volcanic Hazard in Indian Ocean: La Réunion Island Case Study, in *Active Volcanoes of the Southwest Indian Ocean: Piton de la Fournaise and Karthala*, edited by P. Bachelery, J.-F. Lenat, A. Di Muro, and L. Michon, pp. 315–326, Springer Berlin Heidelberg, Berlin, Heidelberg, 2016.
- Del Negro, C., Cappello, A., Neri, M., Bilotta, G., Herault, A. and Ganci, G.: Lava flow hazards at Mount Etna : constraints
- 670 imposed by eruptive history and numerical simulations, *Scientific Reports*, 3(3493), 1–8, doi:10.1038/srep03493, 2013.
- Oehler, J. F., Labazuy, P. and Lénat, J. F.: Recurrence of major flank landslides during the last 2-Ma-history of Reunion Island, *Bull. Volcanol.*, 66(7), 585–598, doi:10.1007/s00445-004-0341-2, 2004.
- Oehler, J. F., Lénat, J. F. and Labazuy, P.: Growth and collapse of the Reunion Island volcanoes, *Bull. Volcanol.*, 70(6), 717–742, doi:10.1007/s00445-007-0163-0, 2008.
- 675 Peltier, A., Bachèlery, P. and Staudacher, T.: Magma transport and storage at Piton de La Fournaise (La Réunion) between 1972 and 2007: A review of geophysical and geochemical data, *J. Volcanol. Geotherm. Res.*, 184(1–2), 93–108,



- doi:10.1016/j.jvolgeores.2008.12.008, 2009.
- Peltier, A., Massin, F., Bachèlery, P. and Finizola, A.: Internal structure and building of basaltic shield volcanoes: The example of the Piton de La Fournaise terminal cone (La Réunion), *Bull. Volcanol.*, 74(8), 1881–1897, doi:10.1007/s00445-012-0636-7, 2012.
- 680 Peltier, A., Villeneuve, N., Ferrazzini, V., Testud, S., Hassen Ali, T., Boissier, P. and Catherine, P.: Changes in the Long-Term Geophysical Eruptive Precursors at Piton de la Fournaise: Implications for the Response Management, *Front. Earth Sci.*, 6(July), 1–10, doi:10.3389/feart.2018.00104, 2018.
- Peltier, A., Ferrazzini, V., Di Muro, A., Kowalski, P., Villeneuve, N., Richter, N., Chevrel, M. O., Froger, J.-L. and Hrysiwicz  
685 A, Gouhier M, Coppola D, Retailleau L, Beauducel F, Boissier P, Brunet C, Catherine P, Fontaine F, Lauret F, Garavaglia L, Lebreton J, Canjamale K, Desfete N, Griot C, Arellano S, Liuzzo M, G. S.: Volcano crisis management during COVID-19 lockdown at Piton de la Fournaise (La Réunion), *Seismol. Res. Lett.*, On line No, 1–15, doi:10.1785/0220200212, 2020.
- Pinkerton, H. and Wilson, L.: Factor controlling the lengths of channel-fed lava flows, *Bull. Volcanol.*, 6, 108–120, 1994.
- Principe, C., Morandi, A., Di Muro, A. and Michon, L.: Volcanological Map of the Plaine des Sables, Piton de la Fournaise,  
690 in *Active Volcanoes of the Southwest Indian Ocean: Piton de la Fournaise and Karthala*, edited by P. Bachelery, J.-F. Lenat, A. Di Muro, and L. Michon, pp. 327–330, Springer Berlin Heidelberg, Berlin, Heidelberg., 2016.
- Rhétý, M., Harris, A. J. L., Villeneuve, N., Gurioli, L., Médard, E., Chevrel, M. O. and Bachèlery, P.: A comparison of cooling-limited and volume-limited flow systems: Examples from channels in the Piton de la Fournaise April 2007 lava-flow field, *Geochemistry, Geophys. Geosystems*, 18(9), 3270–3291, doi:10.1002/2017GC006839, 2017.
- 695 Richter, N., Favalli, M., De Zeeuw-Van Dalfsen, E., Fornaciai, A., Da Silva Fernandes, R. M., Pérez, N. M., Levy, J., Victória, S. S. and Walter, T. R.: Lava flow hazard at Fogo Volcano, Cabo Verde, before and after the 2014–2015 eruption, *Nat. Hazards Earth Syst. Sci.*, 16(8), 1925–1951, doi:10.5194/nhess-16-1925-2016, 2016.
- Roult, G., Peltier, A., Taisne, B., Staudacher, T., Ferrazzini, V., Di Muro, A. and Group, and the O.: A new comprehensive classification of the Piton de la Fournaise eruptions spanning the 1986–2011 period. Search and analysis of eruption precursors  
700 from a broad-band seismological station., *J. Volcanol. Geotherm. Res.*, 241–242, 78–104, doi:10.1016/j.jvolgeores.2012.06.012, 2012.
- Rowland, S. K., Harris, A. J. L. and Garbeil, H.: Effects of Martian conditions on numerically modeled, cooling-limited, channelized lava flows, *J. Geophys. Res.*, 109, E100101, doi:doi.org/10.1029/2004JE002288, 2004.
- Rowland, S. K., Garbeil, H. and Harris, A. J. L.: Lengths and hazards from channel-fed lava flows on Mauna Loa, Hawaii,  
705 determined from thermal and downslope modeling with FLOWGO, *Bull. Volcanol.*, 67, 634–647, 2005.
- Staudacher, T., Ferrazzini, V., Peltier, A., Kowalski, P., Boissier, P., Catherine, P., Lauret, F. and Massin, F.: The April 2007 eruption and the Dolomieu crater collapse, two major events at Piton de la Fournaise (La Réunion Island, Indian Ocean), *J. Volcanol. Geotherm. Res.*, 184(1–2), 126–137, doi:10.1016/j.jvolgeores.2008.11.005, 2009.
- Staudacher, T., Peltier, A., Ferrazzini, V., Di Muro, A., Boissier, P., Catherine, P., Kowalski, P., Lauret, F. and Lebreton, J.:  
710 Fifteen Years of Intense Eruptive Activity (1998–2013) at Piton de la Fournaise Volcano: A Review, in *Active Volcanoes of*



- the Southwest Indian Ocean: Piton de la Fournaise and Karthala, edited by P. Bachelery, J.-F. Lenat, A. Di Muro, and L. Michon, pp. 139–170, Springer Berlin Heidelberg, Berlin, Heidelberg., 2016.
- Tarquini, S. and Favalli, M.: Uncertainties in lava flow hazard maps derived from numerical simulations: The case study of Mount Etna, *J. Volcanol. Geotherm. Res.*, 260, 90–102, doi:<https://doi.org/10.1016/j.jvolgeores.2013.04.017>, 2013.
- 715 Tilling, R. I. and Dvorak, J. J.: Anatomy of a basaltic volcano, *Nature*, 363(6425), 125–133, doi:[10.1038/363125a0](https://doi.org/10.1038/363125a0), 1993.
- Tsang, S. W. R., Lindsay, J. M., Kennedy, B. and Deligne, N. I.: Thermal impacts of basaltic lava flows to buried infrastructure: Workflow to determine the hazard, *J. Appl. Volcanol.*, 9(1), 1–18, doi:[10.1186/s13617-020-00098-w](https://doi.org/10.1186/s13617-020-00098-w), 2020.
- Vergnolle, S. and Bachèlery, P.: Résultats de datations sur bois carbonisés prélevés sur le massif de la Fournaise (île de La Réunion), Observatoire Volcanologique du Piton de la Fournaise, unpublished internal report., 1982.
- 720 Villeneuve, N.: Apports multi-sources à une meilleure compréhension de la mise en place des coulées de lave et des risques associés au Piton de la Fournaise: Géomorphologie quantitative en terrain volcanique., Institut de Physique du Globe de Paris., 2000.
- Villeneuve, N. and Bachèlery, P.: Revue de la Typologie des Eruptions au Piton de la Fournaise, Processus et Risqué Volcaniques Associés, *Cybergeo*, doi:[doi.org/10.4000/cybergeo.2536](https://doi.org/10.4000/cybergeo.2536), 2006.
- 725 Vlastélic, I., Di Muro, A., Bachèlery, P., Gurioli, L., Auclair, D. and Gannoun, A.: Control of source fertility on the eruptive activity of Piton de la Fournaise volcano, La Réunion, *Sci. Rep.*, 8(1), 1–7, doi:[10.1038/s41598-018-32809-0](https://doi.org/10.1038/s41598-018-32809-0), 2018.
- Walker, G. P. L.: Lengths of lava flows, *Philos. Trans. R. Soc. London*, 274, 107–118, 1973.
- Walker, G. P. L.: Three Hawaiian Caldera: An origin through loading by shallow intrusions?, *J. Geophys. Res. Solid Earth*, 93(B12), 14773–14784, doi:[10.1029/JB093iB12p14773](https://doi.org/10.1029/JB093iB12p14773), 1988.
- 730 Wright, R., Garbeil, H. and Harris, A. J. L.: Using infrared satellite data to drive a thermo-rheological/stochastic lava flow emplacement model: A method for near-real-time volcanic hazard assessment, *Geophys. Res. Lett.*, 35(19), 1–5, doi:[10.1029/2008GL035228](https://doi.org/10.1029/2008GL035228), 2008.



735 **Figures and Tables:**

**Figure 1:**

a) La Réunion island (© Google Earth) where the green line delineates the two volcanoes: Piton des Neiges (PN) to the northwest and Piton de la Fournaise (PF) to the southeast.

b) General map of Piton de la Fournaise showing the eruptive fissures as mapped up to end of 2019 (blue lines) and the buildings (in black) with the main municipalities and main roads (in brown - RN2 is the national road). The main three rift zones: north 120° (N120), northeast (NERZ) and southeast (SERZ) and the two volcanic zone: Puy Raymond Volcanic Alignment (PRVA) and South Volcanic Zone (SVZ) are delineated by the dashed red lines as suggested in Bachelery (1981) and Michon et al. (2015). The yellow contour outlines the Enclos depression that is separated in three regions by the dashed yellow lines: the Enclos Fouqué (EF), the steep slopes “Grandes Pentés” (GP) and the eastern lower part “Grand-Brûlé” (GB). The background is the hill-shade of LiDAR DEM from IGN – released in 2010 and coordinates are within system WGS84-UTM 40S. Buildings and roads are from BD TOPO® IGN.

740

745

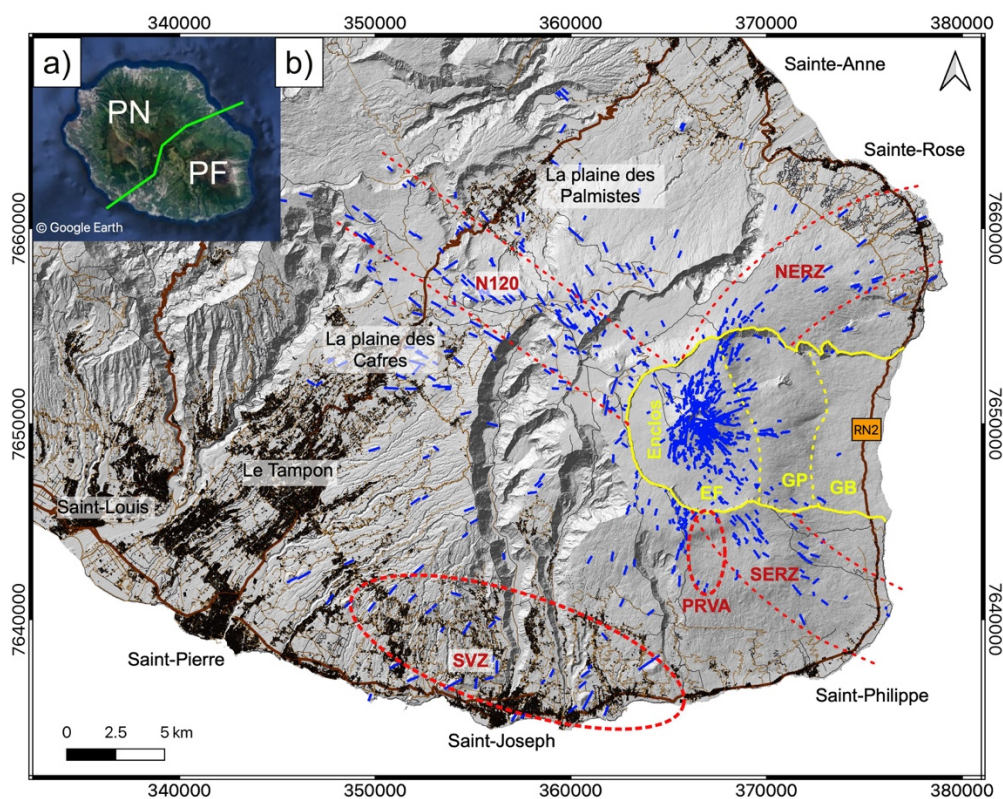
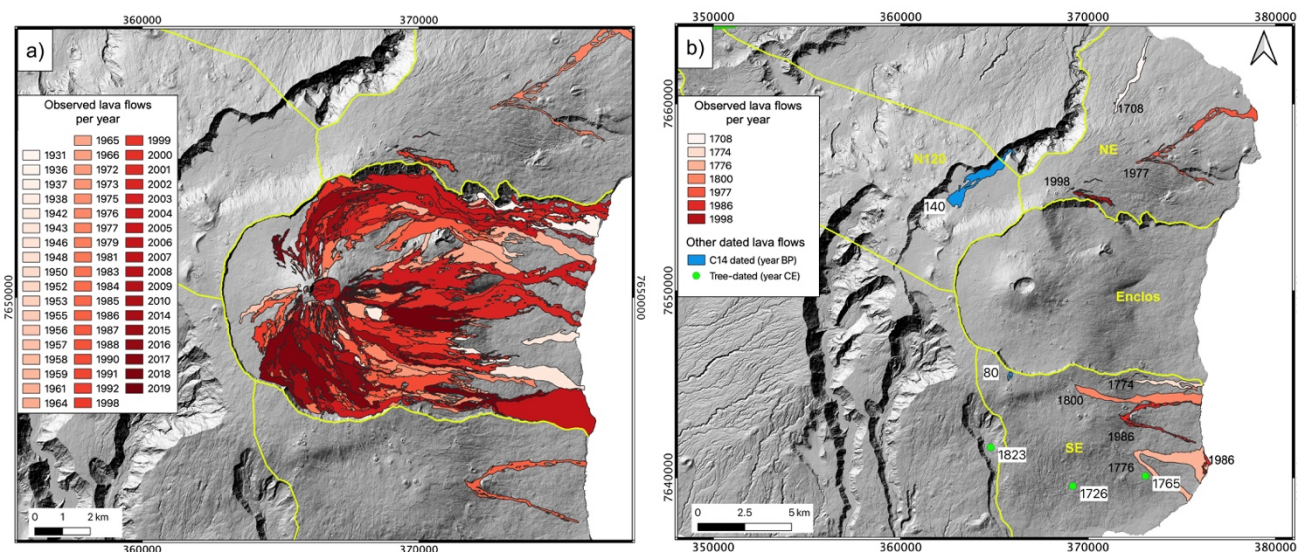




Figure 2: Maps of the lava flows considered in this study.

- 750 a) Lava flows inside the Enclos since 1931 (date from which the lava flow mapping has been well recorded) up to end  
of 2019 from pale to dark red (see Derrien, 2019).
- b) Lava flows outside the Enclos since 1708 and until end of 2019 including i) observed flows (white to red) (see Michon  
et al. 2015): ii) not observed but mapped and dated lava flows (in blue and numbers indicate the year before BP for  
755 C14 dated flows – see Vergnolle and Bachèlery, 1982) and iii) tree-dated lava flows -not mapped (green dots, numbers  
indicate the calendar year for flows - Albert et al. 2020). The yellow lines represent the limits between the regions we  
consider. The background is the hill-shade of LiDAR DEM from IGN – released in 2010.



760



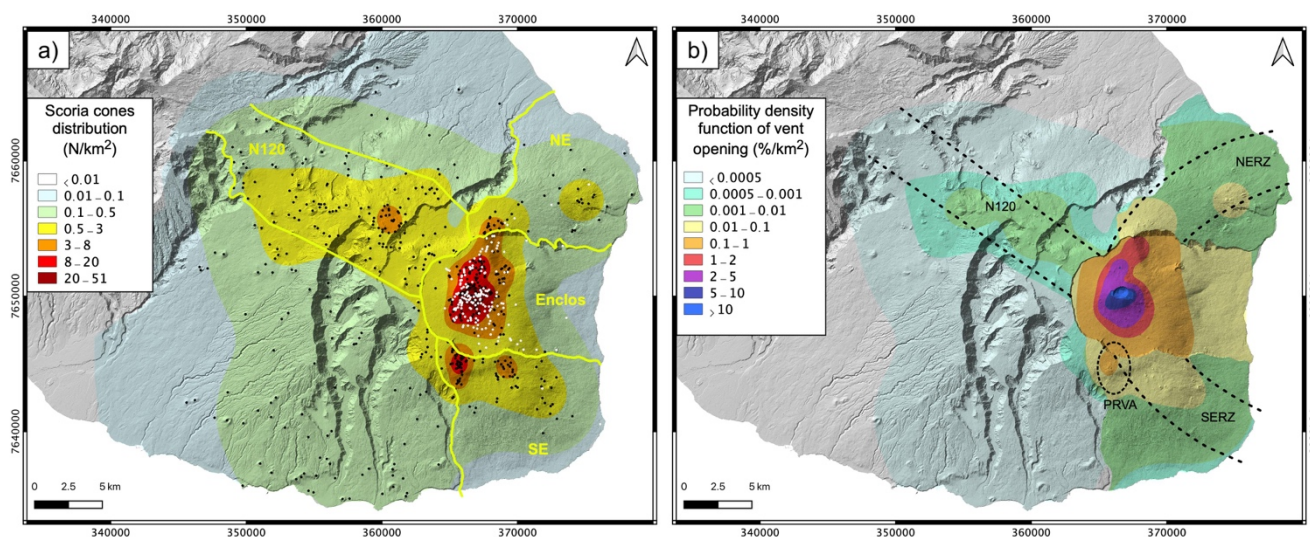
765 **Figure 3:**

a) **Distribution and density (in Number/km<sup>2</sup>) of scoria cones (black dots) on Piton de la Fournaise based on available inventory (OVPF database). In black are scoria cones older than 1931 and in white are the vents from 1931 to the end of 2019. In total they are 726 vents. The yellow lines represent the limits between the regions we considered to estimate probability of vent opening and compute the hazards maps: the Enclos, southeast (SE), northeast (NE), and north 120° (N120) Rift Zones.**

b) **Probability density function of vent opening (in %/km<sup>2</sup>). The dashed lines outline the rift zones to the N 120° (N120), to the northeast (NERZ) and to the southeast (SERZ) as well as the Puy Raymond volcanic alignment (PRVA) – (Bachèlery 1981; Michon et al. 2015).**

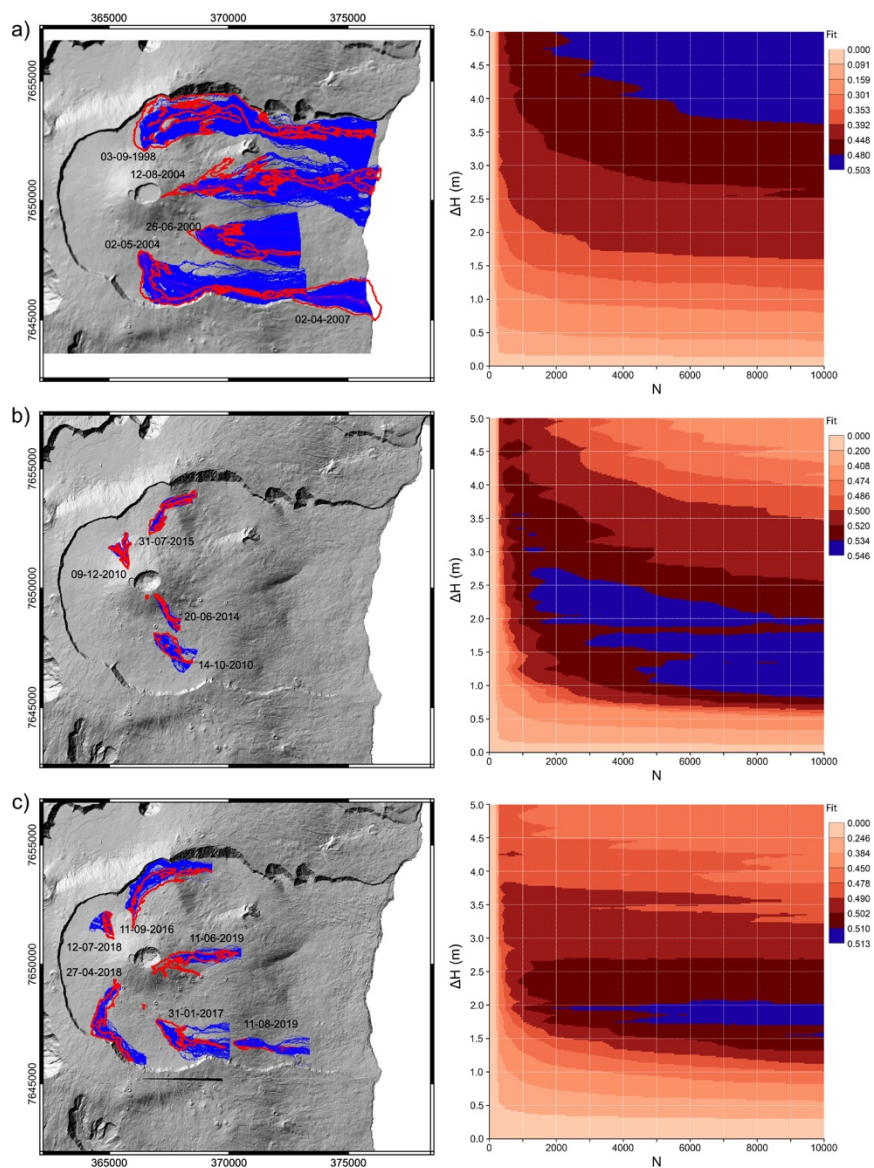
**The green line represents the limit of Piton de la Fournaise with Piton des Neiges. The background is the hill-shade of LiDAR DEM from IGN – released in 2010.**

775





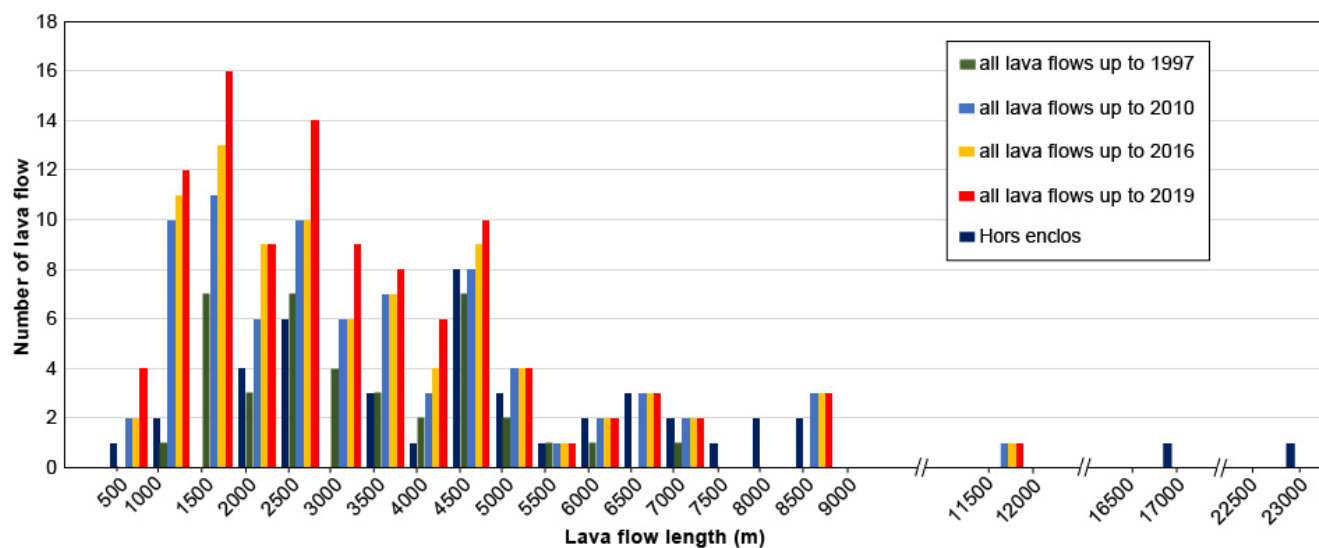
780 **Figure 4: DOWNFLOW calibration for a selected set of lava flows for the three time periods: a) on the 25 m resolution 1997 DEM; b) on the 2010 LiDAR DEM, c) on the 2016 DEM produced from Pleiades. To the left, the maps show the lava flow contours in red and the best DOWNFLOW simulations in blue. To the right, the best fit distribution over the  $\Delta h - N$  space (best-fit parameter range are in dark red and blue).**



785



**Figure 5: Frequency distribution of the lava flow length (by step of 500 m) at Piton de la Fournaise (La Réunion) for lava flows within the Enclos since 1931 and up to 1997, 2010, 2016 and 2019; and for all mapped flows outside the Enclos.**

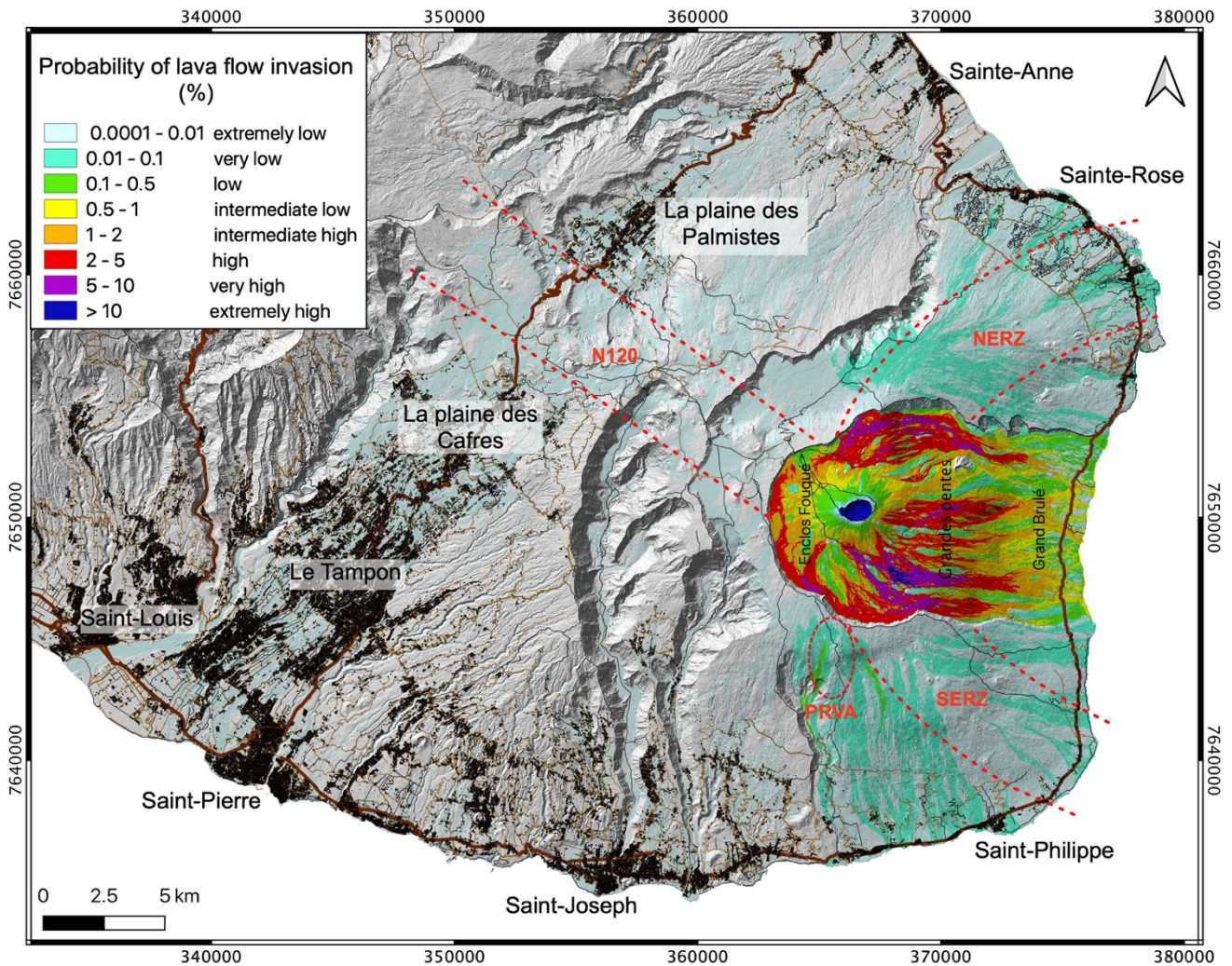


790

795



800 **Figure 6: Lava flow hazard map of Piton de la Fournaise. Probability of lava flow invasion is given as percentages and is color coded from extremely low (<0.01 %) to extremely high (>10 %). Black polygons and grey lines represent the buildings and roads, respectively (municipalities are indicated) and white lines are the touristic trails. The green line represents the limit of Piton de la Fournaise with Piton des Neiges. The background is the hill-shade of LiDAR DEM from IGN – released in 2010. Buildings and roads are from BD TOPO® IGN.**

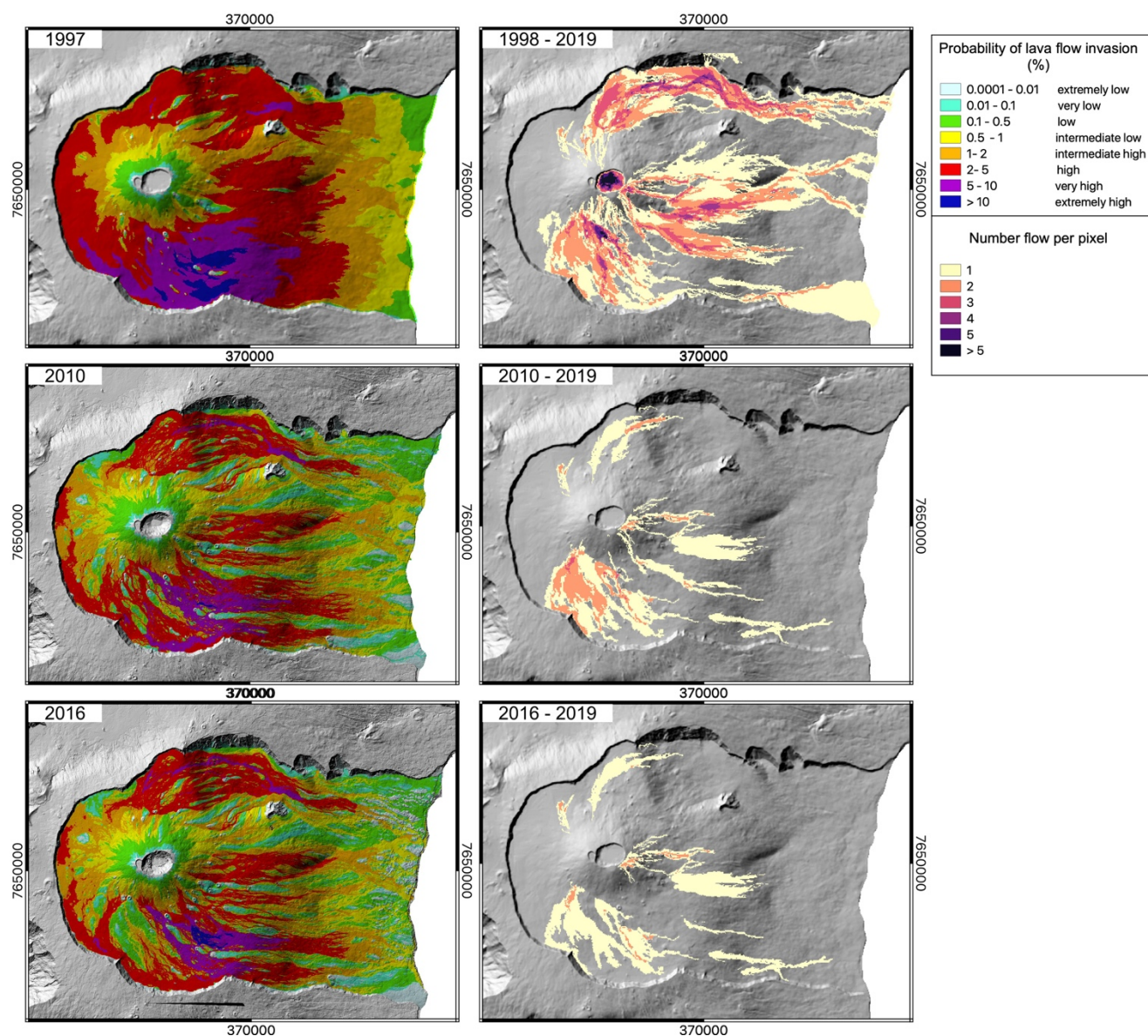




805 **Figure 7: Evolution of the lava flow hazard maps within the Enclos. To the left: the hazard maps are made on the DEM from 1997, 2010 and 2016, respectively, with the corresponding calibration (Fig. 4) and appropriated dataset since 1931 up to the corresponding date (Table 3, Fig. 5).**

**To the right: maps of accumulation of lava (in number of flows per pixel) from the time of the DEM acquisition up to end of 2019.**

810





815 **Table 1: Number of lava flow and statistic of recurrence and relative occurrence probability (see Table S1 for inventory).**

Region	N. lava flows	Time interval (years)	Recurrence time (year)	N. lava flows per year (year <sup>-1</sup> )	Relative occurrence probability (%)
Summit craters	47	88	1.87	0.534	23.55
Enclos w/out craters*	148	88	0.59	1.682	74.16
<b>Inside Enclos**</b>	<b>195</b>		<b>0.45 (5.4 months)</b>	<b>2.216</b>	<b>97.87</b>
SE	9	290	32.22	0.031	1.37
NE	5	311	62.20	0.016	0.71
N120	1	209	209.00	0.005	0.21
<b>Hors Enclos ***</b>	<b>15</b>		<b>20.73</b>	<b>0.048</b>	<b>2.13</b>
Total	210			2.3	100.0

\*Enclos includes the Enclos Fouqué, Grandes Pentes and Grand-Brûlé, except the summit craters area

820 \*\**Inside Enclos* includes the whole Enclos with the summit craters. Lava flows are counted since 1931 up to the end of 2019.

\*\*\**Outside Enclos* lava flows are divided by region south of the caldera (SE), north (NE) and along the N120 rift zone (N120) (see Figure 2), #Time interval corresponds to the time between the oldest considered dated lava flow up to the end of 2019.

825



**Table 2: Scoria cone distribution divided by regions**

<b>Region</b>	<b>N. vents</b>	<b>Fraction of vents (%)</b>
Summit craters	27	3.72
Enclos w/out craters*	300	41.32
<b><i>Inside Enclos**</i></b>	<b>327</b>	<b>45.04</b>
SE	98	13.50
NE	49	6.75
N120	142	19.56
Rest of the volcano	110	15.15
<b><i>Hors Enclos***</i></b>	<b>399</b>	<b>54.96</b>
Total	726	100

\*Enclos includes the Enclos Fouqué, Grandes Pentes and Grand-Brûlé, except the summit craters area

830 \*\**Inside Enclos* includes the whole Enclos with the summit craters. Lava flows are counted since 1931 up to the end of 2019.

\*\*\**Outside Enclos* lava flows are divided by region south of the caldera (SE), north (NE) and along the N120 rift zone (N120) (see Figure 2),



835 **Table 3: Lava flow relative occurrence probability and scoria cone distribution within Enclos for the 1931-1997, 1931-2010, 1931-2016 and 1931-2019 periods**

Region	N. lava flows	Time interval (years)	Recurrence time (year)	N. lava flows per year (year <sup>-1</sup> )	Relative occurrence probability (%)	N. Scoria cones	Fraction of Scoria cones (%)
since 1931 up to 1997							
Summit craters	31	66	2.13	0.47	27.93	3	3.41
Enclos w/out craters	80	66	0.83	1.21	72.07	85	96.59
Total	111			1.68	100.00	88	100
since 1931 up to 2010							
Summit craters	46	79	1.72	0.58	26.74	9	5.81
Enclos w/out craters	126	79	0.63	1.59	73.26	146	94.19
Total	172			2.18	100.00	155	100
since 1931 up to 2016							
Summit craters	47	85	1.81	0.55	25.82	10	6.10
Enclos w/out craters	135	85	0.63	1.59	74.18	154	93.90
Total	182			2.14	100.00	164	100
since 1931 up to 2019							
Summit craters	47	88	1.87	0.53	22.71	10	5.38
Enclos w/out craters	160	88	0.55	1.82	77.29	176	94.62
Total	207			2.35	100.00	186	100